NOTE TO USERS

Page(s) not included in the original manuscript and are unavailable from the author or university. The manuscript was scanned as received.

x-xi

This reproduction is the best copy available.

UMI®

Fabrication of Magnesium Matrix Composites Using a Spontaneous Infiltration Technique

By

HUIQIANG CHEN

Department of Mining, Metals and Materials Engineering

McGill University

Montreal, Canada

November 2002

A thesis submitted to the Faculty
of Graduate Studies and Research
in partial fulfillment of the
requirements of the degree of
Master of Engineering

Your file Votre référence
ISBN: 0-612-88348-5
Our file Notre référence
ISBN: 0-612-88348-5

Abstract

A new process was developed to fabricate particulate metal matrix composites (MMCs). The process involves two steps: (1) forming a particulate porous compact, and (2) introducing molten magnesium or magnesium alloy (AZ91) into the channel network by a spontaneous infiltration technique.

A uniform distribution of SiC particulates in magnesium matrix was achieved. Microsegregation existed in composites when the particle size of reinforcement was 38 μm and 22 μm, however, when the particle size of reinforcement was 12 μm, the microsegregation was eliminated.

The interfacial reaction between SiC and Mg studied by Scanning Electron Microscopy (SEM), microanalysis and X-Ray Diffraction (XRD) techniques showed that, Mg reacted with Si or SiO_2 to form Mg_2Si, Mg_2Si was present at the surface of SiC after precipitation, resulting in improved wettability between Mg and SiC. As a result of this interfacial reaction, the infiltration process became spontaneous. The infiltration process was related to the infiltration temperature, SiC particle size and matrix chemistry. Increasing the infiltration temperature, decreasing the particle size of SiC resulted in more successful infiltration.

Mechanical testing conducted on composites revealed that the hardness and Ultimate Tensile Strength (UTS) of composites increased with the decrease of particle size of SiC and corresponded to an increase of the volume fraction of SiC.

Résumé

Un nouveau procédé a été développé pour la fabrication de matériaux composites à matrice métallique. Ce procédé se divise en deux étapes: (1) formation d'une préfore poreuse; (2) introduction du magnésium ou alliage magnesium (AZ91) liquide dans les conduits de la préforme poreuse par une technique d'auto infiltration.

Une distribution uniforme des particulesde SiC dans la matrice magnésium est obtenue. Présence de microségrégation est observé dans les composites lorsque la grandeur des particules de renforcement est de 38 μm et 22 μm. cependant, pour des particules de renforcement de 12 μm, la microségrégation est éliminée.

Les réactions interfaciales entre le SiC et le Mg ont été étudiées par spectroscopie à énergie dispersive et diffraction des rayons-X. Les résultats démontrent que le Mg réagit avec le Si ou le SiO_2 pour former Mg_2Si. Le revêtement de Mg_2Si à la surface des particule de SiC est responsable pour l'amélioration de la mouillabilité entre Mg et SiC. L'infiltration spontannée est obtenue grâce à cette couche de réaction. Le procédé d'infiltration est fontion de la temperature d'infiltration, la granulométrie du renforcement (SiC) et de la composition chimique de la matrice. Le taux d'infiltration augmente en fonction de la température et de la diminution de la taille des particules.

Les essais mécaniques ont demontés que la dureté et la résistance ultime à la traction augmentint avec la diminution de la taille des particules de SiC, i.e., l'augmentation de la fraction volumique de SiC.

ACKNOWLEDGEMENTS

I would like to express my sincere gratitude to Prof. R.A.L Drew for his guidance, valuable advice and supervision throughout the entire project. Especially, I wish to thank him for the academic and personal freedom that he encouraged and allowed during my thesis work.

I would like to thank all the specialists and lab technicians for providing me with all the required tools, equipments and suggestions that make it is easier to perform all the different tests during this work. Special thanks go to Helen Campbell, Robert Paquette, Ray Langlois, Slawomir Poplawski and Florence Paray. I appreciate very much the help of Abdelbaset Elwazri with the shear punch testing, and the cooperation and assistance of the workshop personnel.

I wish to thank all my fellow graduate students who made my stay at McGill filled with fun, excitement and learning. To Mathieu, Claudia and the whole ceramic group, thank you so much for sharing your time and space with me. You have all made my time of research here at McGill a memorable one.

Finally, I have to extend my greatest respect and appreciation to my family, Dad, my older sister and my brothers for their unconditional love and support. My proudest achievements, including this work, have all been the result of their infinite encouragement. I would like to take the opportunity to remind my oversea family that I love them forever. And last and not at least, my love and dedication to Ye.

Table of Contents

List of Figures

List of Tables

Chapter 1

Introduction

Modern technology has placed increasing demands on materials. This need for better materials is particularly acute in the area of dynamic structures, where not only high strength is required, but also lightweight. The efficiency of dynamic structures such as aircraft, high speed manufacturing machinery, power generating equipment, and aerospace equipment could be affected by an improvement in the structural efficiency of the materials. A key problem in designing in these structures pertains to the square-cube relationship: that is, the strength and stiffness of a structure increase with the square of the linear dimension, whereas the weight increases with the cube of the linear dimension. In order to maintain the stiffness and strength, high strength and stiffer materials are required [1]. With the advent of Metal Matrix Composites (MMCs), it is now possible to increase the stiffness and hardness of the metallic matrices by the addition of stiffer and harder reinforcements.

Metal Matrix Composites (MMCs) are homogeneous materials created by the synthetic assembly of metal and reinforcement to obtain specific characteristics and properties [2].

Metal Matrix Composites (MMCs) have a series of advantages that are very important in the utilization of structural materials. These advantages relate to the same metallic properties that have led to the general primacy of metal alloys for use in dynamic engineering structures [1]. The development aims of light metal matrix composites can be summarized as follows [3]:

- Increase in yield strength, ultimate tensile strength and fatigue strength at room temperature whilst maintaining minimum values of ductility or toughness;
- Increase in hot strength, fatigue strength and creep resistance at elevated temperatures compared to conventional materials;
- Reduction in the coefficient of the thermal expansion of light metal alloys to values comparable with steels;
- Improvement in the stability of light metal to temperature changes, improvement in damping behavior;
- Improvement in the wear resistance through addition of hard materials;
- Improvement in weight specific properties (strength and Young's modulus).

The early work on composites considered continuous fiber reinforcement, and while work in this area continues, it was soon apparent that the cost of continuous fiber, complex fabrication routes, and limited fabricability, would restrict their use to those applications requiring the ultimate in performance. This led to the development of discontinuously reinforce composites, particularly short staple Al_2O_3 fiber and SiC whisker reinforced composites. Particle reinforced light metals, with their potential as low cost, high modulus and strength, high wear

resistance, and easily fabricated material, are just reaching the commercial production stage [4].

The particulate reinforcement can lead to isotropic material properties, since the material is symmetrical across the three orthogonal planes. Strength of the particulate reinforced composites normally depends on the diameter of the reinforcement, interparticle spacing, and the volume fraction of the reinforcement [1].

Since most ceramics are available as particles, there is a wide range of potential reinforcement for particulate reinforced composites. The choice depends on the application required, the matrix alloy system and the method chosen for production [3].

A variety of processes have been and are being developed for manufacture of particulate reinforced composites by either liquid, including casting or infiltration processes or compaction of powders involving liquid phase sintering. Liquid-phase fabrication of composite materials has long been considered an economically viable casting process [5]. Nowadays, some composites are available to meet a strength specification [4].

MMCs are routinely included as candidate materials for primary and secondary structural applications. However, simply having the best engineered material with extraordinary material strength, stiffness, and environmental resistance is no guarantee. The availability and affordability of MMCs remains a significant barrier to their acceptance in engineering [6].

During the development of MMCs, significant advancements have made on the fundamental science and technology front, including a basic understanding of composite behavior, reinforcement/matrix interfaces, surface coating, manufacturing processes, and thermal mechanical processing. Subsequently, the technology experience benefited the late development of high temperature intermetallic matrix composites [6].

Magnesium is one of the lightest structural materials known in engineering. With its about 35% lower density compared with aluminum, it carries tremendous potential for engineering applications requiring high specific mechanical properties. However, due to the low elastic modulus, insufficient strength at room temperature and elevated temperature, insufficient creep resistance and very high coefficient of thermal expansion, its applications for critical engineering materials are limited [7]. In recent years, SiC reinforced magnesium based composites have been manufactured. SiC/Mg composites show higher stiffness and strength that makes magnesium MMCs a possibility for engineering applications [8].

The aim of this thesis is to investigate the feasibility of producing magnesium based composites. In particular it, focuses on liquid infiltration method to produce magnesium composite reinforced with SiC particulates. *Chapter 2* briefly outlines the basic materials, design considerations and fabrication processes used in the production of Mg/SiC composites. The experimental procedure is given in *Chapter 4*. *Chapter 5-6*, the results and discussion are presented. Finally, conclusions and recommendations for future work are given in *Chapter 7.*

Chapter 2

Literature Review

2.1 Metal Matrix Composites (MMCs)

Metal matrix composites consist of a matrix and one or more reinforcing phase. The reinforcing constituent is normally a ceramic, although occasionally a refractory metal is preferred. The matrix constituent is usually a light metal, such as aluminum, magnesium and titanium. The reinforcement incorporates into the matrix normally increasing its strength, as they are stronger than the matrix alloys and imparting some special properties to the composites [5].

According to the type of reinforcement, The MMCs can be divided into three categories [9]:

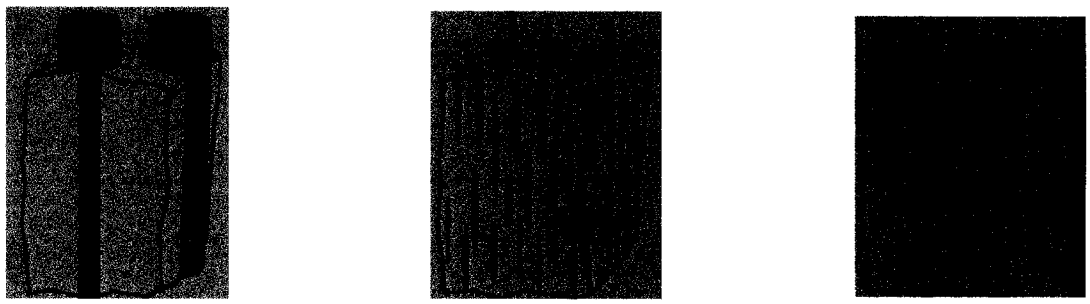

Monofillaments Whiskers/Staple Fibres Particulate

Figure.2.1 Schematic depiction of the three types of MMCs

Earlier, the high cost of manufacturing MMCs compared to most monolithic materials restricted their applications to aerospace and defense industries, and very few engineering application in automotive and consumer goods industries appeared viable, until the pioneering work by Toyota Motor Company in 1983 of a selectively reinforced squeeze cast composite diesel piston. Subsequently, Honda announced a steel-reinforced composite connecting rod. Since then, several automotive and consumer goods industries have attempted to exploit the advantages of cast MMCs in automotive parts [10].

Nowadays, more and more metal matrix composites have been applied in aerospace, automotive and construction industries. *Table 2.1* [4] listed some commercially available metal matrix composites.

Table 2.1 Typical properties of some commercially available metal matrix composites

Composite*	YS+ ($MN\ m^{-2}$)	UTS ($MN\ m^{-2}$)	Elongation %	Supplier
Wrought				
Al-Mg2Si				
6061/Al2O3/10p (T6)	296	338	7.5	Duralcan, Alcan
6061/Al2O3/15p (T6)	317	359	5.4	Duralcan, Alcan
6061/Al2O3/20p (T6)	359	379	2.1	Duralcan, Alcan
6061/Al2O3/20p (T6)	305	330	3.4	Comral 85, Comalco
6061/SiC/15p (T6)	342	364	3.2	Cospray, Alcan
6061/SiC/15p (T4)	405	460	7.0	DWA‡
6061/SiC/20p (T4)	420	500	5.0	DWA‡
6061/SiC/25p (T4)	430	515	4.0	DWA‡
Al-Cu				
2014/Al2O3/10p (T6)	483	517	3.3	Duralcan, Alcan
2014/Al2O3/15p (T6)	476	503	2.3	Duralcan, Alcan
2014/Al2O3/20p (T6)	483	503	1.0	Duralcan, Alcan
2014/SiC/15p (T6)	466	493	2.0	Cospray, Alcan
2618/SiC/12p (T6)	460	532	3.0	Cospray, Alcan
2124/SiC/17.8p (T4)	400	610	5 to 7	BP
2124/SiC/25p (T4)	490	630	2 to 4	BP
2124/SiC/20p (T4)	405	560	7.0	DWA‡
Al-Zn-Mg				
7075/SiC/15p (T651)	556	601	3.0	Cospray, Alcan
7049/SiC/15p (T6)	598	643	2.0	Cospray, Alcan
7090/SiC/20p (T6)	665	735	2.0	DWA‡
Al-Li				
8090/SiC/13p (T4)	455	520	4.0	Cospray, Alcan
8090/SiC/13p (T6)	499	547	3.0	Cospray, Alcan
8090/SiC/17p (T4)	310	460	4 to 7	BP¶
8090/SiC/17p (T6)	450	540	3 to 4	BP¶
Cast				
Ai-Si				
356/SiC/10p (T61)	287	308	0.6	Duralcan, Alcan
356/SiC/15p (T61)	329	336	0.3	Duralcan, Alcan
356/SiC/20p (T61)	336	357	0.4	Duralcan, Alcan
380/SiC/10p (F)	245	332	1.0	Duralcan, Alcan
380/SiC/20p (F)	308	356	0.4	Duralcan, Alcan
Mg-Al-Zn				
AZ91/SiC/9.4p	191	236	2.0	Dow
AZ91/SiC/15.1p	208	236	1.0	Dow
AZ61/SiC/20p	260	328	2.5	Dow

- Composite designation: matrix/reinforcement/volume fraction of particles.

+ 0.2% offset yield stress.

‡ Composite Specialities Inc, CA.

¶ British Petroleum.

2.1.1 Reinforcement and matrix metal selection

The purpose of the matrix in a composite material is to combine the reinforcing particles into a monolithic material for shaping into the required geometrical form and dimensions, as well as to take up and distribute external loads with the material bulk. In addition, the matrices protect the reinforcing phase against external effects: mechanical damage, erosion, and corrosion caused by the surrounding medium. A variety of metals, such as Al, Li, Mg, Ti, Cu, Zn, Fe and Pb, and almost all the structural alloy systems have been considered as matrix materials for MMCs. The most common alloys employed are those of aluminum, titanium and magnesium, as well as intermetallic compounds. Titanium has been extensively studied with the perspective of high temperature applications. Nickel and nickel-based superalloys are also possible candidates for high temperature applications when weight limitation is not a primary objective.

A wide range of reinforcement materials with different properties is available in industry. The choice depends on the method chosen for production and on the matrix alloy system [3]. In general, the requirements are:

- low density [3];
- high elastic modulus, high compressive and tensile strength [3,9];
- good chemical stability [3];

- mechanical and chemical compatibility [3];
- ease of fabrication [3,9];
- reproducibility or consistency of properties [9];
- resistance to damage or abrasion [9];
- economical [3, 9].

Inorganic reinforcing materials can only fulfill these demands. Often only ceramic particles or fibers or carbon fibers are used to reinforce metal [3, 9].

Obvious, the candidates for light metal matrices for composite materials are the easily workable, conventional alloys [3].

2.1.2 Characteristics of magnesium and SiC

With plentiful resource, the lowest density and easily machined, magnesium is becoming most studied metal matrix for applications on aerospace and automotive in future.

The characteristics of pure magnesium are [11]:

- Density: 1.74 g/cm^3,
- Melting Point: 650 °C,
- Coefficient of Thermal Expansion (CTE) (20-500 °C): 29.9 μm/°C

Table 2.2 Typical mechanical properties of unalloyed magnesium at 20 °C

Form and section	Tensile strength (MPa)	0.2% tensile yield strength (MPa)	0.2% compressive yield strength (MPa)	Hardness	
				HRE	HB(a)
Sand Cast, 13mm diam	90	21	21	16	30
Extrusion 13mm diam	165-205	65-105	34-55	26	35
Hard rolled sheet	180-220	115-140	105-115	48-54	45-47
Annealed sheet	160-195	90-105	69-83	37-39	40-41

(a) 500 kg load, 10 mm diam ball

Table 2.3 Typical mechanical properties of magnesium alloys at room temperature:

Alloy	Tensile strength MPa	Compressive yield strength MPa	Shear strength MPa	Hardness HR(c)
AZ81A-T4	275	83	125	55
AZ91D	250	160	140	70

Silicon carbide powder matches well the requirement for reinforcement. The characteristics of silicon carbide are [12]:

- •low density (3.1-3.2g/cm^3)
- •high strength (Flexural strength: 550 MPa; Compressive strength: 3900 MPa)
- • low thermal expansion (4.0 x 10^{-6}/°C);
- • high hardness (2800 kg/mm^2);
- • high elastic modulus (410GPa);
- • low cost and availability;
- • superior chemical inertness.

2.2 Fabrication of Metal Matrix Composites

Generally, Metal Matrix Composites (MMCs) have been produced by squeeze casting, powder metallurgy (P/M), stirring method and infiltration (including vacuum, pressureless and pressure) method.

2.2.1 Squeeze casting

Squeeze casting is a process that involves the solidification of a molten metal in a closed die under imposed high pressure. Other terms used to describe the same or similar processes are liquid metal forming, extrusion casting and pressure crystallization [13]. It is a common and efficient method to produce light metals or light metal alloys composites [7, 13-18].

The squeeze casting process involves several steps [13]:

i) A suitable dieset is installed on the bed of a hydraulic press. The dieset is preheated to the required temperature. During the heating-up period, the dieset is usually sprayed with a commercial graphite lubricant.

ii) A metered quantity of molten metal is poured into an open female die cavity. Then, an upper male die or punch is lowered, coming into contact with molten metal.

iii) The pressure is applied shortly after molten metal begins to solidify and is maintained until all the molten metal has solidified.

iv) The upper punch returns to its original position and the casting is ejected.

Two different types of squeeze casting technologies have been used in net-shape composite, based upon different approaches to metal metering and metal movement during die filling. These methods have been named " direct" and " indirect" casting [13, 14].

Direct squeeze casting (DSC) is characterized by a direct pressure applied on the casting without any gating system. *Figure 2.2* schematically shows the procedure for direct squeeze casting [13].

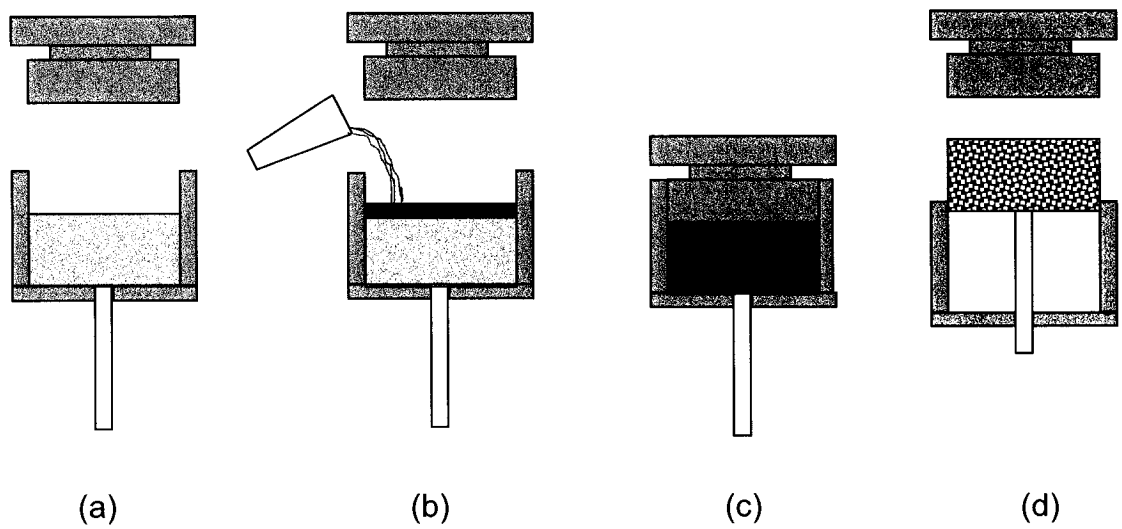

Figure. 2.2 Schematic diagram of the squeeze casting processes (a) Step 1, preheat, lubricating tools. (b) Step 2, transfer melt into die cavity. (c) Step 3, solidify melt under pressure. (d) Step 4, eject casting.

The major advantages of direct squeeze casting are as follows:

1) it is the most efficient and effective route to produce near net shape products [7, 13-18].

2) components have no gas porosity and shrinkage porosity, making them sound and of good quality [14].
3) the microstructure of components is easily controlled [13] and fine grain sizes are attained [13].
4) higher mechanical properties are achieved [13].
5) economic [7,14,18].

In the indirect process, molten metal is injected into the die cavity with a large diameter piston, which is also used to apply pressure during freezing [13]. *Figure 2.3* schematically shows the process [13].

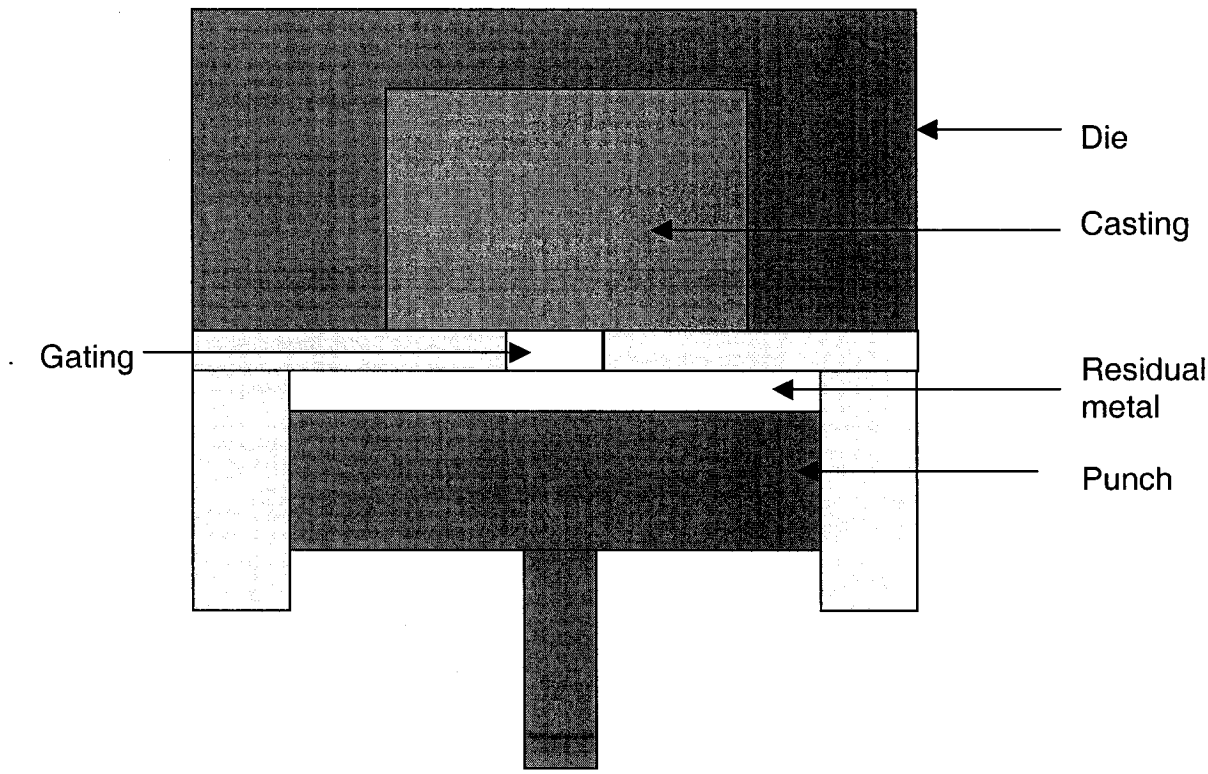

Figure 2.3 Schematic diagram of indirect squeeze casting process.

The advantage of indirect technique is that, due to the presence of a gating system, a highly accurate external metering is not necessary. Variations in metal volume are adjusted in the gate [13].

Compared with direct squeeze casting, the major disadvantages of indirect squeeze casting are follows:

i) Materials wastage [13,14];
ii) Difficult to produce high strength composites [14].

Although indirect squeeze casting had some disadvantages, it had been commercialized by UBE industries in Japan to produce high quality automobile parts [14].

In squeeze casting, both direct and indirect, there are a number of parameters that generally influenced the soundness and quality of composites [13,14,17]. The vital parameter in the process is pouring temperature and pressure. Also, in some case, the preheating temperature also plays an important role in optimizing the process [19].

2.2.2 Stirring casting

Due to low cost, high productivity, and near net shape capability, stirring casting is a preferred choice for the fabrication of metal matrix composites (MMCs) [20]. Recently, composites based on magnesium and magnesium alloys have been fabricated by a fluxless casting method [8, 20-21].

Stirring process involves the following steps [8, 20-21]:

i) superheating magnesium chips with silicon carbide powder to 750°C under inert gas;

ii) stirring the molten metal at 450-470 rpm for 5 minutes; in order to facilitate the incorporation and uniform distribution of the SiC particulates in the metallic matrix;

iii) pouring molten composite through a 10 mm nozzle in the graphite crucible;

iv) using two linear inert gas flow to break up the molten stream;

v) finally, the molten composite being deposited on a circular shaped metallic substrate.

Figure 2.4 shows schematically the processes.

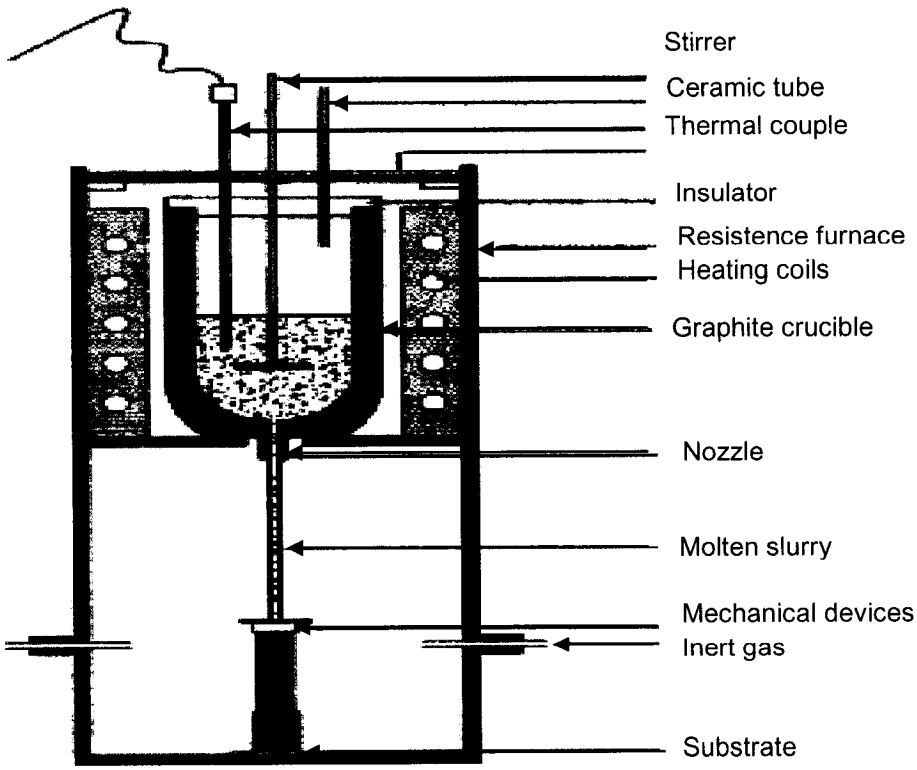

Figure 2.4 Schematic diagram of stirring casting methods

2.2.3 Powder metallurgy (P/M)

Powder metallurgy is one of the most popular methods to produce metal matrix composites (MMCs) [4, 7,10, 22] and *Figure 2.5* [7] shows the flow chart for production.

The powder metallurgy route has several features [4]:

- It allows essentially any alloy to be used as matrix.
- It also allows any type of reinforcement to used because reaction between the matrix and reinforcement can be minimized by using solid state processing.
- Non-equilibrium alloys can be used for the matrix by using rapidly solidified material.
- High volume fractions of reinforcement are possible, thus maximizing the modulus and minimizing the coefficient of thermal expansion (CTE).

However, the powder metallurgy route has some major disadvantages: It involves handling large quantities of highly reactive, potentially explosive powder and the manufacturing procedure is relatively complex [4].

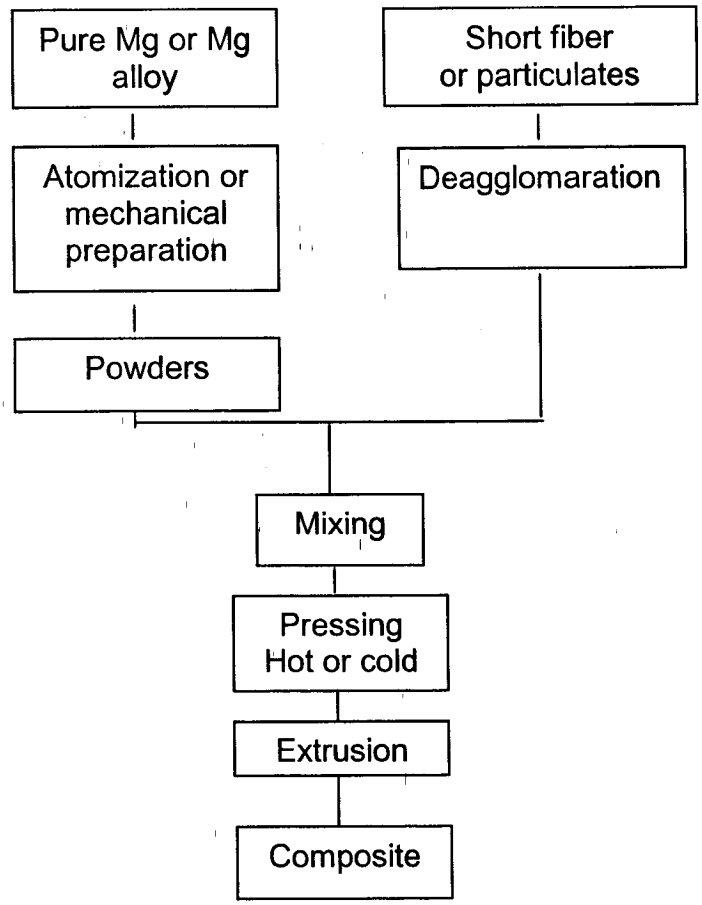

Figure 2.5 Production steps for powder metallurgy MMCs.

P/M technology allows the use of alloys with supersaturated or metallic phases. The alloys are free from segregation problems as is often observed after conventional solidification. Examples of extensively investigated conventional magnesium matrix alloys as AZ91, MSR, QE22, AZ31, ZK60 and ZC63 [3].

2.2.4 Infiltration Technique

The basic infiltration process consists of impregnating a porous ceramic perform of fibers or particles with the matrix alloy, followed by solidification of the infiltrant within the fine pores of the preform. Infiltration processes have been applied to MMCs for several years [10]. However, there have been few studies involving spontaneous infiltration to the fabrication of magnesium matrix composites.

Kaneda and Choh [23] attempted to apply spontaneous infiltration to fabrication of SiC particle reinforced magnesium matrix composites. The process involved: 1) choosing SiO_2 as infiltration promotion agent, 2) mix SiO_2 with reinforced powder, 3) melt magnesium and spontaneously infiltrate into the powder mixture. Their results indicated that, the SiO_2 content was necessary for completion of spontaneous infiltration; also, the SiO_2 content varied for various SiC_p diameters. The result was shown in *Figure 2.6*.

The process has many advantages for fabricating magnesium MMCs, such as a relatively low process temperature, short incorporation time and no defects [23].

2.2.5 Other processes

In magnesium base composites, except for the process mentioned above, semisolid forming [24, 25] and the rotation-cylinder [26] method have also been applied.

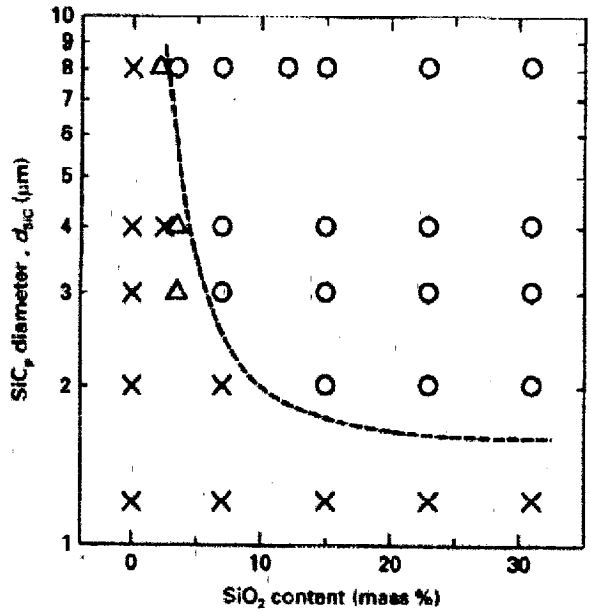

Figure 2.6 Effects of SiO_2 content and reinforcement particle diameter on spontaneous infiltration. (O) – completed infiltration, (Δ) – incompleted infiltration, (x) – no infiltration.

2.2.6 Secondary processing

Mg/SiC_p composites obtained from stirring casting processes or other methods are usually machined and then hot extruded at 350°C at a reduction ratio by a hydraulic press [8, 20-21]. After secondary processing, the mechanical properties of composites are improved since fine particle size was achieved [19].

2.3 Infiltration Dynamics

2.3.1 The wettability between metal and ceramic

The wettability of a solid by a liquid is characterized in terms of the angle of contact that the liquid makes on the solid. The contact angle, θ, is obtained from a balance of interfacial tensions according to the Young-Dupré equation [10]:

$$\gamma_{lv}.\cos\theta + \gamma_{ls} = \gamma_{sv} \qquad (2.1)$$

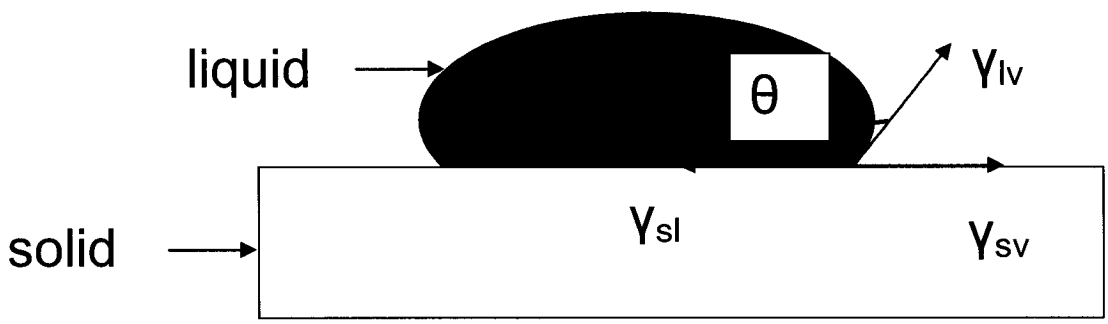

Figure. 2.7 Schematic diagram of wettablity between molten metal and ceramic

where γ_{lv}, γ_{ls}, and γ_{sv} are the interfacial tensions at the boundaries between liquid (l), solid (s), and vapor (v). Here, γ represents the force needed to stretch an interface by a unit distance (or, equivalently, energy required to create a unit surface area of a given interface, provided that, in the case of γ_{sv}, mechanical distortion and strains are negligible). The condition $\theta < 90°$ indicates that the solid is wet by the liquid, and $\theta > 90°$ indicates nonwetting, with the limits $\theta = 0$ and $\theta = 180°$ defining complete wetting and complete nonwetting, respectively.

Due to the poor wettabilty between the metal and ceramic, for melt intrusion of a porous ceramic perform, a pressure threshold must be overcome. This is controlled by the capillary phenomenon described by the Young-Laplace equation:

$$P_c = 2\gamma_{lv} \cos \theta / r \qquad (2.2)$$

Where P_c is the capillary pressure required to effect melt intrusion into a capillary of uniform radius r, and, γ_{lv} and θ are the surface tension and wetting angle [10].

Extensive works to improve the wettability between ceramics and metals in metal matrix composites processing have been done. Leon and Drew [27] processed metal matrix composites by wetting assisted infiltration using metal-coated reinforcements. Ceramic powders, such as Al_2O_3 and SiC, were coated by Cu, Ni using an electroless plating method. The coated powder would improve the wettability between ceramic (Al_2O_3 and SiC) and metal matrix (Al and Al alloys). Hojo et al [28,29] coated Al_2O_3 by Ni and/or W powder to improve the wettability between Al_2O_3 and Ni/Cu. It indicated that molten Ni and Cu were easily infiltrated into the pores, giving dense composites of Al_2O_3 – Ni and Al_2O_3 –Ni – Cu systems. Also, modification of the matrix chemistry by addition elements such as Mg, Li, and Na [10,30] is a common method to improve the wettability between ceramics and metals.

2.3.2 Improving wettability by chemical reaction

Generally, interfacial reactions between metals and ceramics involve adsorption, dissolution and redox-type chemical reactions. Chemical reaction can occur during liquid state processing depending upon such fabrication

parameters such as temperature, time, gas atmosphere and chemical compositions of both phases. These interfacial reactions generally lead to a reduction in the solid-liquid interfacial energy and thereby improved the wettability and interface bonding (physical and chemical bonding, mechanical keying, residual stress and interfacial dislocation density). The extent of reinforcement surface degradation also depended upon the extent of chemical interaction between the reinforcement and metal. The thermodynamic and kinetic effects of reaction-induced wettability under dynamic conditions relevant to pressure casting of composites were usually represented in terms of pressure threshold and incubation time [10].

The incubation time decreased with increasing temperature. At lower infiltration temperature, an incubation time was observed in the infiltration profiles, and, it was believed to relate to mass transfer; Also, the wettability would increased with increase of infiltration time [31, 32].

In spontaneous infiltration processing, the reaction between ceramics and metals played an important role [2]. In an Al/ceramic system (85-90% Al_2O_3, 15-10% SiO_2), the wetting angle reached 90° at 1000 °C, but dropped to 45 - 50° in the temperature range 1200 – 1250 °C [2]. XRF was used to analyze the elemental distribution and revealed that the interaction zone is poor in silicon, whereas the melt adjacent to the contact surface contained a large amount of free silicon. This is due to the reaction occurring that it was reduction occurred between SiO_2 and Aluminum,

$$Al + SiO_2 = Al_2O_3 + Si \qquad (2.3)$$

Although the chemical reaction improved the wettability, the properties of composites were generally degraded [33].

In magnesium-based composites, a number of researchers have worked on the interaction between magnesium and reinforcement [8, 20-21, 34-39]. It was shown that, since free silicon and silica (SiO_2) covered the surface of Silicon Carbide (SiC), these materials would react with magnesium at temperatures above 700 °C. The possible reactions are as follows:

$$2Mg + Si = Mg_2Si \qquad (2.4)$$

$$2Mg + SiO_2 = 2MgO + Si \qquad (2.5)$$

2.4 Infiltration Kinetics

The infiltration kinetics of liquid metals in fiber preforms and particulate compacts have been studied in TiC/Al [321, 32], Al_2O_3 [40, 41] and SiC/Al [42].

The effects of pore size on the infiltration kinetics in TiC/Al system have been studied [31, 32]. The infiltration profiles indicated that 1) the curves were not completely parabolic with infiltration time at low temperature; 2) there was a incubation period at low temperature; 3) the contact angle decreased with increase of temperature and time; 4) activation energy increased with increasing pore size.

Liegbusi and Yang [40] studied the mechanism of porosity nucleation during pressure infiltration casting of Al_2O_3/Al composites. The results showed the

applied pressure increased as the contact angle increases, also, the addition of the specific alloying elements (Mg, Cu) significantly accelerated the infiltration process due to a reduction of the contact angle.

Hu et al [41] analyzed the infiltration kinetics based on Darcy's Law and assumptions in Al_2O_3/Al composite. It was found that a parabolic relationship did exist between the infiltration time and infiltration depth during the infiltration process whilst an incubation period is required to activate the infiltration. Darcy's Law was modified as follows:

$$X = \xi (t^{1/2} - t_0^{1/2}),\ T > \text{or} = t_0 \qquad (2.6)$$

Where X was the infiltrated depth, t was infiltration time, t_0 was the incubation time required to activate infiltration and ξ was the infiltration rate.

Yamauchi and Nishida [42] studied the effects of preform temperature on the infiltration process in SiC_w/Al composites. The results showed that at low pre-heating temperature, the molten Al did not reach the bottom of the preform. However, when the temperature reached the melting temperature of Al, infiltration was complete.

The theoretical analysis of infiltration through porous ceramic perform was complicated owing to spatial variation of channel (pore) size in the preform, the connectivity and tortuosity of the porous network, the segregation of solutes and discontinuous deposition of reaction products at the preferred sites on the reinforcement [10].

2.5 Microstructure of SiC/Mg composites

The most important aspect of the microstructure is the distribution of the reinforcing particulates, and this depends on the processing and fabrication route involved.

In composites processed by the molten metal mixing methods, the distribution of the reinforcement is influenced by several factors [4]:

1. distribution in the liquid as a result of the mixing.
2. distribution in the liquid after mixing but before solidification.
3. redistribution as a result of solidification.

The distribution during mixing will obviously depend on the mixing process used, and it is essential to produce as uniform a distribution as possible without any gas entrapment. After mixing, and before solidification, the particulates will segregate due to gravity. The segregation is a function of particle size and shape. Finally, the solidification process will strongly influence the distribution of the reinforcement as shown in *Figure. 2.8* [4].

Also, another important aspect of microstructure is the matrix grain size. As a result of increasing the presence of SiC particulates, magnesium matrix grain size was refined to some extent. Comparing the grain structure of unreinforced AZ91 alloy and AZ91/SiC composite prepared under same condition, Luo [44] reported that SiC has an obvious effect on the matrix microstructure. The grain size of magnesium is reduced by approximately a factor of 3 in the case of AZ91/SiC composite. The grain refinement in the composites was due to the

combined effect of heterogeneous nucleation of primary magnesium on SiC particulate and restricted growth of magnesium grains during solidification. Similar results were observed by other researchers [8, 20-21].

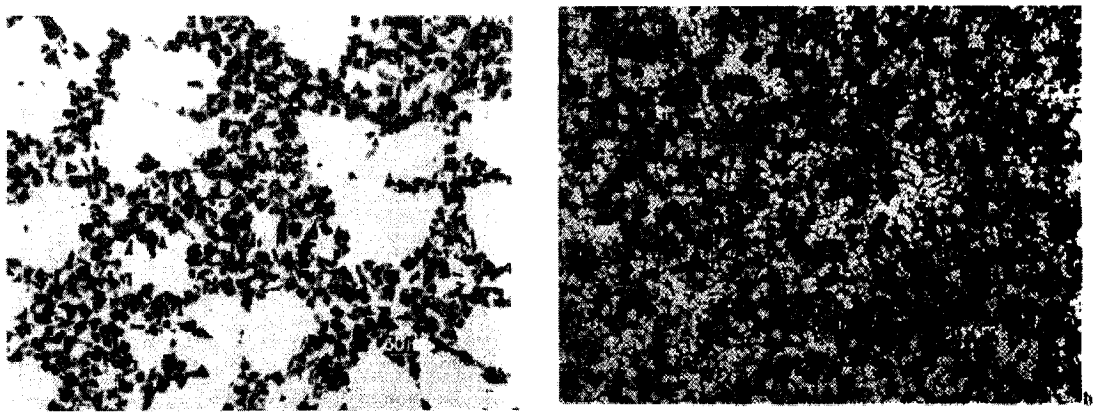

a) b)

Figure.2.8 Influence of solidification conditions on particle distribution: a) slow rate, b) high rate of cooling

Figure 2.9 [23] shows the photomicrographs of composites obtained by the spontaneous infiltration process for the Mg/SiC_p composites. SiO_2 (3μm, 7wt%) acted as infiltration agent. SiC_p homogeneously distributed in the magnesium matrix and few pores were observed even though the SiC particulates were fine and no agitation was applied.

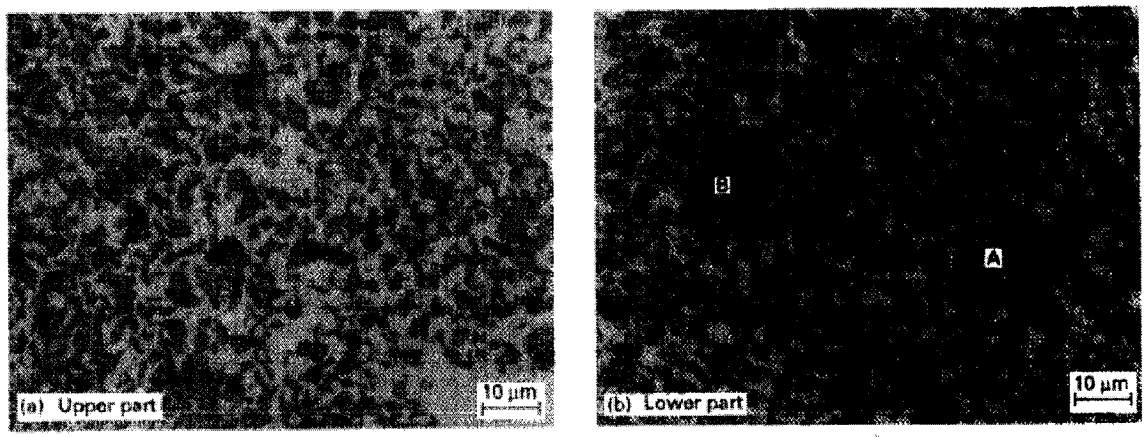

Figure 2.9 Microstructure of composites fabricated by the spontaneous infiltration process for the Mg/SiC_p composites. (a) upper part, (b) lower part

These photographs indicated that two compounds were formed during processing (marked A and B in *Figure 2.9 b*). SEM and EPMA analysis confirmed that phase A and B were Mg_2Si and MgO [23].

2.6 Interfacial region

2.6.1 General

An interface is a region of significant chemical composition change that constitutes the bond between the matrix and the reinforcement for transferring of loads between these components of the composite [33].

The interface plays a crucial role in transferring the load efficiently from the matrix to the reinforcement. The strengthening and stiffening of composites are dependant on the load transfer across the interface. High bond strength is required at the interface for effective load transfer. A strong bond is usually formed with the reaction between the matrix and reinforcement, the reaction

product determining the nature of the bond. A brittle reaction product at the interface makes the composite crack at lower strains [44].

It is known that in many cases there is a large different in the coefficient of thermal expansion (CTE) between the matrix and reinforcement. When the MMC is cooled from an elevated temperature (e.g. fabrication) to room temperature, misfit strains arise due to differential thermal contraction at the interface. These strains induce thermal residual stresses which may be higher that the yield stress of the matrix. Thermal stresses may be accommodated by the generation of new dislocation at the interface. Therefore, after cooling the composite, its mechanical, electrical and thermal properties can change due to changes in the interfaces [19].

The importance of studying the interface region in composites stems from two main factors: (1) the interface occupies a very large area in composites, and (2) in general, the reinforcement and the matrix will form a system that is not in thermodynamic equilibrium. A strong adherent interface is a critical prerequisite for a good composite structure. The nature and quality of the interface are determined by factors both intrinsic to the reinforcement and matrix materials as well as extrinsic. In MMCs a moderate amount of chemical interaction between the reinforcement and matrix improves wetting, assists liquid-phase fabrication of the composite and enhances the strength of the interface [5].

In metal matrix composites (MMC), the free energy characterizes bonding between two components of the composite. The work of adhesion W_a can be expressed as:

$$W_a = \gamma_m + \gamma_c - \gamma_i \qquad (2.7)$$

Where γ_m is the surface energy of the metallic matrix and γ_c is the surface energy of the ceramic reinforcement, γ_i is the free energy per unit area of an interface. If the W_a is positive, then there is attractive interaction between the two components. The higher the values of W_a, the more stable is the interface [45].

Based on the type of chemical reaction occurring between the reinforcement and matrix, a classification of interfaces has been developed. The three classes proposed are [33]:

Class I, reinforcement and matrix are mutually nonreactive and insoluble;
Class II, reinforcement and matrix are mutually nonreactive but soluble;
Class III, reinforcement and matrix react to form compound(s) at the interface.

It may be assumed that class III interfaces may also exhibit mutual solubility between the matrix and reinforcement as well as the product phases [33].

This classification is useful in describing the thermodynamic stability of the interface because each class is consistent with thermodynamic phase equilibriums. This system also describes the relative chemical stability of a composite interface .A class I interface is characteristic of a stable matrix/reinforcement, whereas a class III is characteristic of a highly unstable matrix/reinforcement interface [33].

To control the extent of the interfacial reaction, common practices include shortening processing time, coating reinforcements with materials of different reactivities, and adding alloying elements to the matrix [44, 46].

2.6.2 Nature of SiC/Mg interface

Due to the high reactivity of magnesium, the interfacial microstructure between the matrix and reinforcement plays an important role in Mg-base composites. The nature of the interface in discontinuously reinforced Mg matrix composite rests with a variety of factors, such as: the composition of the matrix alloy, the composition and the nature of the reinforcement, the fabrication techniques, and the thermal treatment conditions applied to the composites.

The SiC/Mg interfacial integrity, assessed in terms of interfacial debonding and the presence of voids is considered being excellent [20,21]. A typical SiC/Mg interface is shown in *Figure.2.10:*

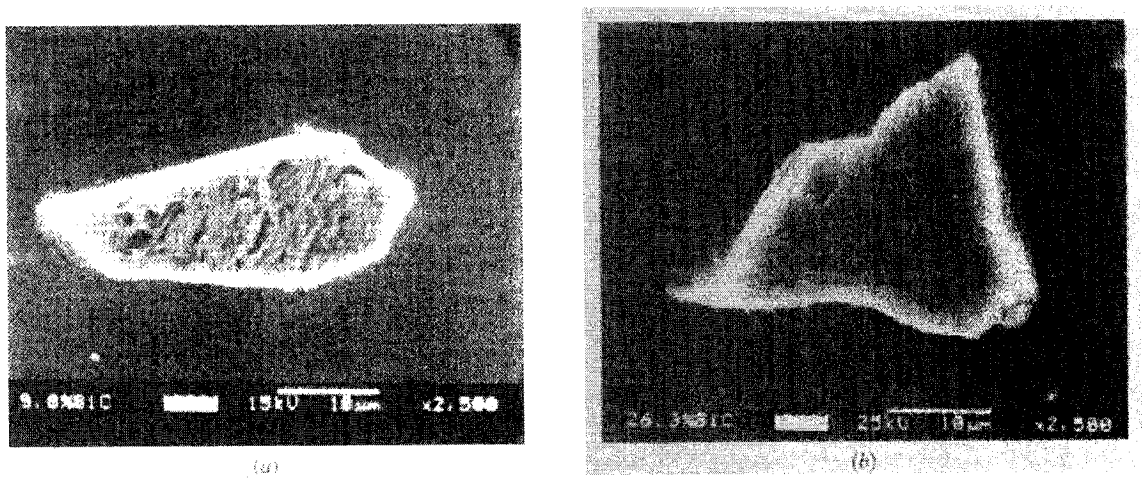

Figure.2.10 Typical interface between the matrix and SiC (a) Mg/SiC/9.8 wt% and (b) Mg/SiC/26.3 wt% composites [21].

INEM and POLLARD [39] investigated Mg-6%Zn, 3%Cu, 0.5%Mn (ZCM630)/SiC interface by transmission electron microscopy (TEM). A typical interfacial microstructure was observed as shown in *Figure 2.11.* The interfacial structure consists of an essentially featureless interface in which matrix and eutectic are in

intimate contact with the particles, it indicates there is no evidence of extensive chemical reaction at the interface. This result is consistent with the work of Cai et al. [34].

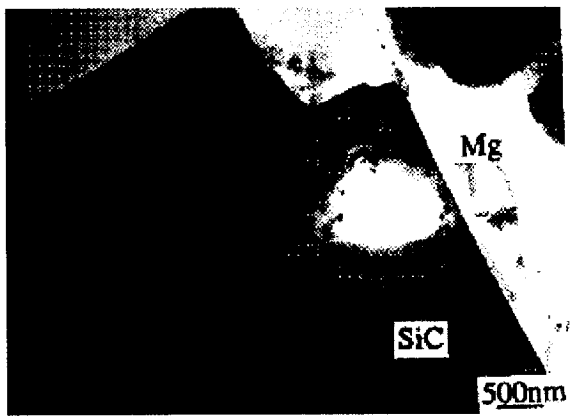

Figure.2.11 TEM micrograph showing the matrix/SiC interface.

However, two different particles at the interface of ZCM630/SiC have been detected and microanalysized by EDX as shown in *Figure. 2.12*

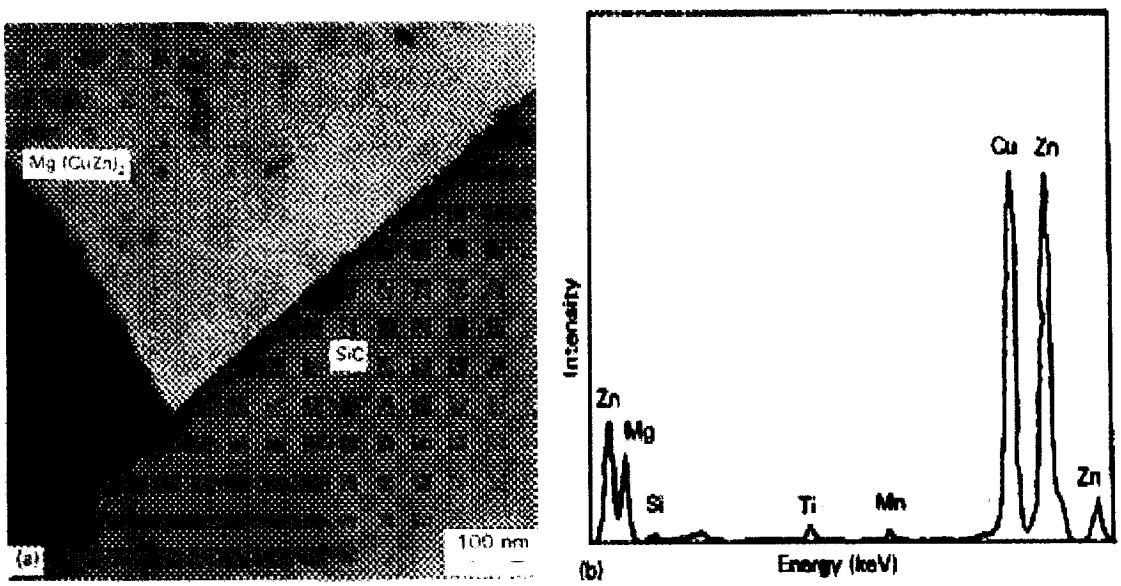

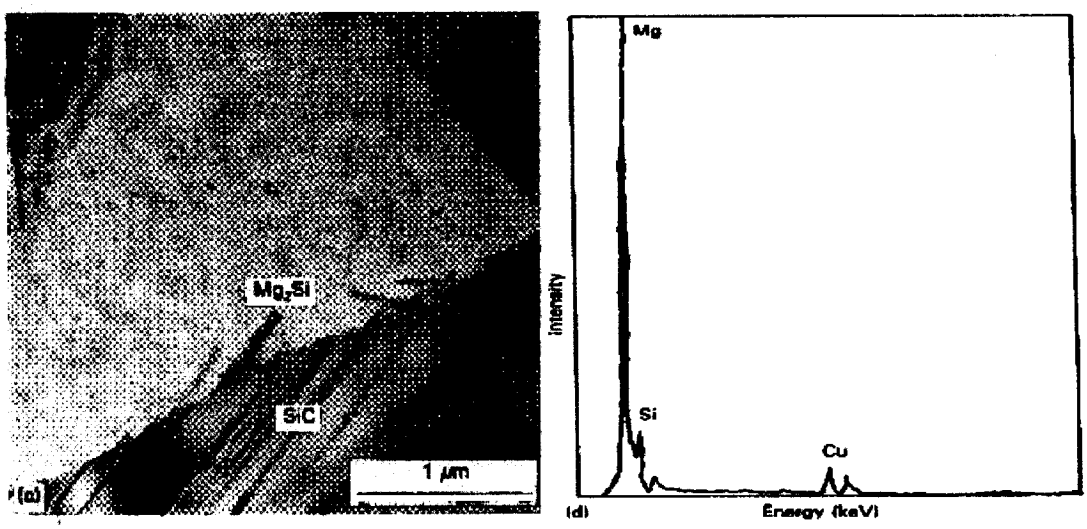

Figure.2.12 (a) TEM micrograph showing eutectic droplets and a massive ternary eutectic phase on SiC particle, (b) EDS analysis of the eutectic phase, (c) Mg_2Si phase on the SiC particle at the interface, and (d) EDS analysis from Mg_2Si phase [39]

From these results, it is believed that during solidification, free Si and SiO_2 from the SiC particle together with Mg form Mg_2Si at the Mg/SiC interface. There are two possible reactions for the formation of Mg_2Si [20,21,39].

$$2Mg + SiC = Mg_2Si \qquad (2.8)$$

$$4Mg + SiO_2 = Mg_2Si + 2MgO \qquad (2.9)$$

The eutectic phase improves the wettability between the matrix and SiC.

The process parameter i.e. temperature affects the interfacial region. Laurent and Jarry [19] investigated the stirring temperature on the AZ91D/SiC interface. It was found, that at 581-588 °C, no evidence of reaction product or erosion of particle surface was observed at the SiC/Mg interface; at a higher temperature of 689 °C, a discontinuous layer of Mg_2Si at the particle/matrix interface was found.

2.7 Dislocation substructure

In MMCs, the large difference between the coefficient of thermal expansion (CTE) of the matrix and the reinforcement results in sufficient stress to generate a high dislocation density at the interface during the solidification and heat treatment. This high stress and consequent dislocation generation around the reinforcement has often been related to good bonding at the interface. A high dislocation and extensive twining around the particles has been observed in magnesium-matrix composite in *Figure 2.13* [39].

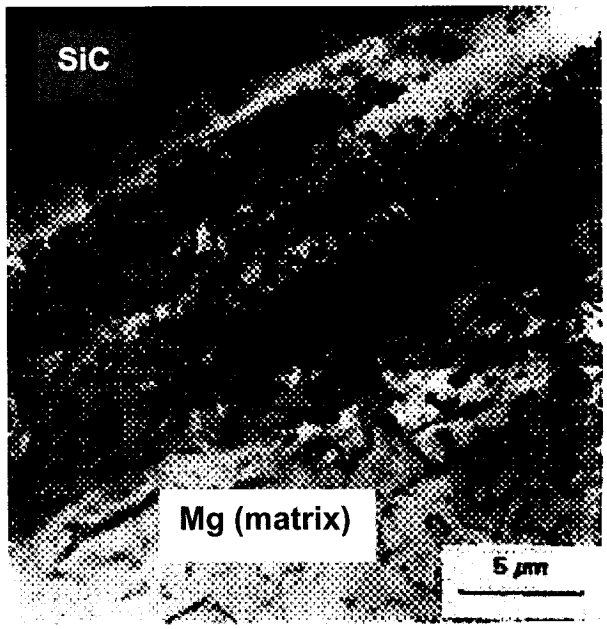

Figure 2.13 A high dislocation density and heavy twining around the SiC particles

2.8 Mechanical properties of Mg-base composites

2.8.1 Hardness

The hardness (microhardness or macrohardness) of SiC/Mg composites increases with an increase in the weight percentage of SiC particulates. This can be attributed to increasing the presence of harder SiC particulates in the matrix, higher constraints to localized matrix deformation during indentation as a result of the increasing presence of SiC particulates, and an increasing ability of SiC particulates to refine the matrix microstructure [21, 43]. Also, a higher dislocation density originating from a strong interface between the particulates and matrix combined with the CTE mismatch contributes to the increase in hardness [39]. *Table 2.4* lists the hardness results of different SiC/Mg composites [21].

Table 2.4 Results of hardness measurements

Material composition, wt-%	Microhardness, HV (25g)		Macrohardness
	Matrix	SiC/Mg interface	HRT15
Mg	47.2	...	40
Mg-7.6SiC	48.9	99	45.3
Mg-14.9SiC	49.1	102	49.5
Mg-26.0SiC	49.9	113	57.6

In order to predict the hardness of SiC/Mg composite, Lim and his co-worker [21] have correlated the bulk hardness (H) of matrix with the weight percentage of SiC particulates (W). The empirical relationship developed is:

$$H = 0.671W + 39.969 \quad (2.10)$$

It should be note that the maximum weight percentage is 26.3% in equation 2.10

2.8.2 Elastic modulus

The elastic modulus of a material represents the relative stiffness of the material within the elastic range and can be determined from a stress-strain curve by calculating the ratio of stress to strain. In Metal Matrix Composites (MMCs), Elastic modulus can also be computed using Halpin-Tsai Equation [21]. That can be expressed as:

$$E_c = \frac{Em(1+2sqVr)}{1-qVr} \qquad (2.11)$$

Where *Ec* and *Em* are the elastic moduli of composite and matrix, *Vr* is the volume fraction of the reinforcement and *s* is the aspect ratio of the reinforcement. q is related to the elastic modulus of reinforcement and matrix which can be expressed as:

$$q = \frac{Er/Em-1}{Er/Em+2s} \qquad (2.12)$$

Where *Er* is the elastic modulus of the reinforcement.

Equation 2.11 indicates that, the predominant factor in controlling the elastic modulus is the volume fraction of reinforcement, and it is insensitive to the particle distribution [4]. Also, casting temperature affects the elastic modulus as well. Hu and Wang [17] investigated the effect of casting temperature on elastic modulus of SiCw/ZK51A composite. The results revealed that the casting temperature had a significant influence on elastic modulus. Raising the casting temperature, the elastic modulus increases; however, above 760 °C, the elastic

modulus decreases to some extent with further increase a casting temperature. *Figure.2.14* shows the dependence of the elastic modulus on casting temperature in a SiCw/ZK51A composite. Therefore, an optimal casting temperature should exist and the SiCw/ZK51A composite, that temperature is about 760 °C.

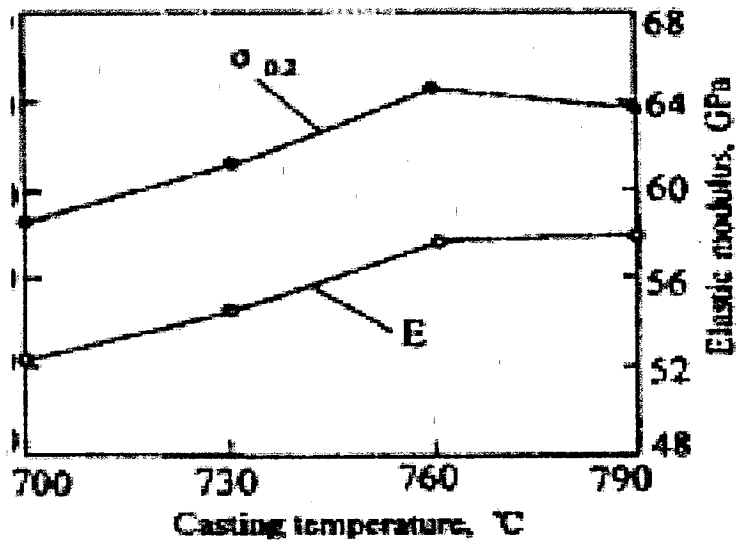

Figure.2.14 Dependence of elastic modulus of SICw/ZK51A (Vf:0.15) on casting temperature

Gupta and his co-workers [8] compared elastic modulus of SiC/Mg composites by calculation and experiments. The results show the experimental values follow the same trend as calculated values, but their magnitude remained lower. One reason for the lower experimental elastic modulus values is a finite amount of non-connected porosity in the composites. The presence of such porosity may adversely affect the elastic response of the materials as a result of reduction in effective load bearing area. They also, reported that elastic modulus of SiC/Mg composites increase with increasing the weight percentage of SiC particulates,

due to the higher elastic modulus of SiC particulates than that of the magnesium matrix.

2.8.3 Elongation

The major limitation in the mechanical properties of composites is the rather limited ductility. The tensile elongation decreases rapidly with the addition of reinforcing particles. Composite failure associates with particle cracking and void formation in the matrix within clusters of particles. Particles fracture is more prevalent in coarser particles due to (i) coarser ceramic particles contain more fracture initiating defects; (ii) the larger the particle is, the more it will be loaded [4].

2.8.4 Strength

Mechanical properties of Mg-based composites are related to the reinforcement, matrix alloy and fabrication technique. Generally, the reinforcement plays an important role on improving mechanical properties [4].

Manoharan and his co-workers [47, 48] concluded that the reinforcement in composites contribute to the strengthening of the composite for two reasons. Reinforcements act as barrier to dislocation motion resulting in an increase in strength. Secondly, the reinforcement develops net internal stress in the matrix. In SiC/Mg composites, the large difference between SiC and Mg in the elastic, plastic and thermal properties results in the development of internal stress. Based on the two contributions outlined above, the total strength, σ_c, can be estimated as:

$$\sigma_c = \sigma_m + \frac{\mu b}{\lambda} + 4.8\mu f\varepsilon \qquad (2.13)$$

Where μ is the shear modulus of the matrix, b is the Burgers vector, λ is the particle spacing, f is the volume fraction of reinforcement, ε is the plastic strain, and σ_m is the mean internal stress, where $\sigma_m = 4\mu f\varepsilon$.

Lim et al. [21] researched the properties of SiC/Mg composites, and reported that an increase in weight percentage of SiC particulates in the magnesium matrix does not affect the 0.2% YS but lowered the UTS and ductility compared with unreinforced Mg. This was attributed to the coupled influence of the presence of a higher volume fraction of porosity and the reduced cavitations resistance of the metallic matrix owing to the combined presence of porosity and SiC particulates.

On the other hand, Luo [43] proposed that the yield strength of the composite material significantly improved over the unreinforced magnesium alloy. However, he found that the UTS of the composite is also lower than that of the matrix alloy. Meanwhile, Saravana and M. K. Surappa [49] have reported that either 0.2% YS or UTS is higher that that of pure magnesium at room temperature.

2.8.5 Facture behavior of SiC/Mg composites

The fracture process in particulates reinforced composites is quite complex, and a quantitative understanding is lacking. Hence different composites maybe dominated by different fracture processes.

Gupta and his co-workers [8, 20-21, 48] analyzed the fracture surface of SiC/Mg composites produced by the stirring cast technique. The results revealed a typical brittle fracture in the case of Mg samples. This was attributed to the HCP

crystal structure of magnesium that restricts slip to the basal plane; In the case of SiC/Mg composites, evidence of extensive plastic deformation adjacent to SiC particulates is indicative of strain accumulation at the SiC/Mg interface and the presence of broken SiC particulates with minimal interfacial debonding indicates a good interfacial bonding occurs between SiC and Mg.

Saravanan and Surappa [49] reported, in the case of Mg-30 vol% SiC_p composite, at elevated temperature, more than one mode of deformation is operative in SiC/Mg composites. At room temperature, extensive SiC particle fracture was observed whereas the matrix exhibits quasi-brittle fracture. Further, at higher temperature, true fracture had occurred by void coalescence and crack bridging between the reinforcement particles.

Chapter3

Objectives

The present work involves several aspects of magnesium-based composites reinforced with SiC particulates. The main objectives are to:

i) establish a novel method for fabricating magnesium based composites, with different particle sizes of SiC;

ii) investigate the effects of particle size of SiC on the resulting composites;

iii) characterize the microstructure of composites in terms of reinforcement distribution, porosity and overall soundness;

iv) identify any interfacial reaction between the matrix and reinforcement;

v) evaluate some of the mechanical properties.

Chapter 4

EXPERIMENTAL PROCEDURE

The present work involves the development of an infiltration technique for fabricating particulate reinforced magnesium and magnesium alloy composites. The experimental work is divided into three steps: 1) setup a new method. 2) fabricate particulate reinforced and magnesium alloy composites by the infiltration technique; 3) perform the microstructural and mechanical characterization of the performed composites. The experimental procedure is shown in *Figure.4.1*. Each of the main steps will be discussed in the following sections.

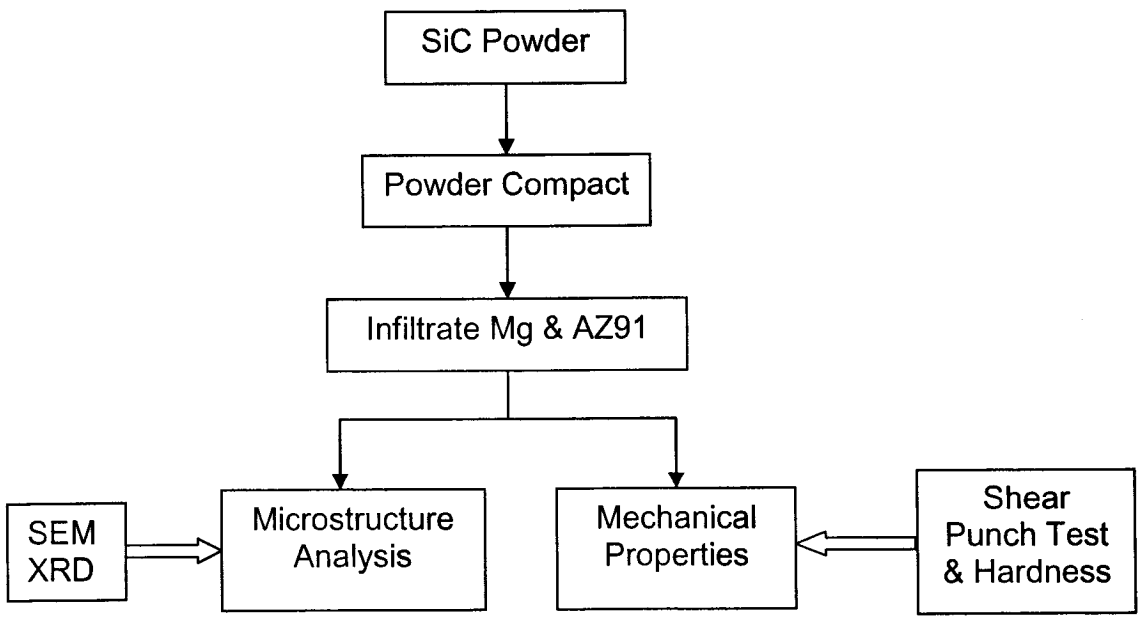

Figure 4.1 Experimental procedure flow chart

4.1 Raw materials

4.1.1 Silicon Carbide (SiC)

The materials employed were pure β-SiC (97%n min., *Superior Graphite Co. Silicon Carbide*) powders. The chemical composition, as reported by the manufacturer, is listed in *Table 4.1*

Table 4.1. Typical chemical analysis for SiC powders

Silicon Carbide	(SiC)	97% min.
Carbon	(C)	0.55~0.71%
Oxygen	(O)	0.19~1.50%
Nitrogen	(N)	0.09~0.13%
Iron	(Fe)	139~473 ppm
Aluminum	(Al)	0~450 ppm

The particle size of SiC employed in the experiment was HSC400 (38 μm), HSC600 (22 μm) and HSC1200 (12 μm). The as received particle size distributions are shown in *Figure 4.2 -4.4.*

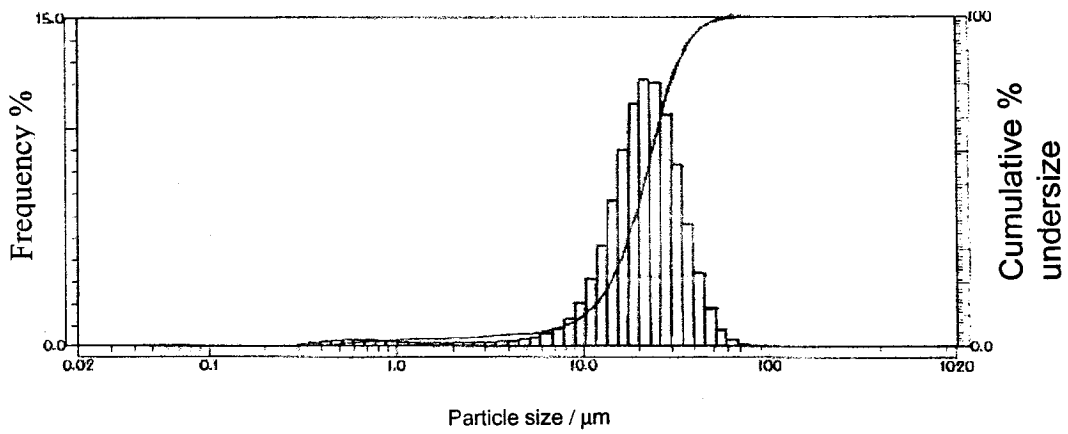

Figure 4.2. Particle distribution as received of HSC400 (38 μm)

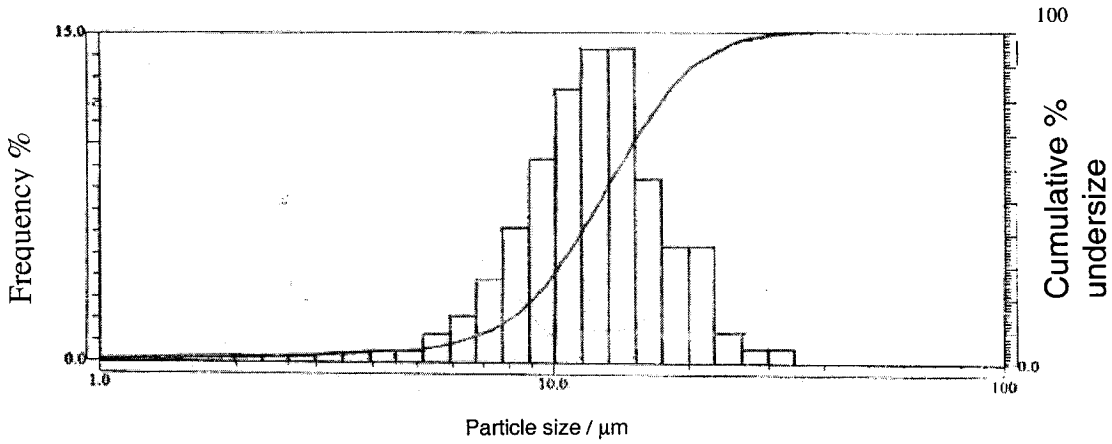

Figure 4.3. Particle distribution as received of HSC600 (22 µm)

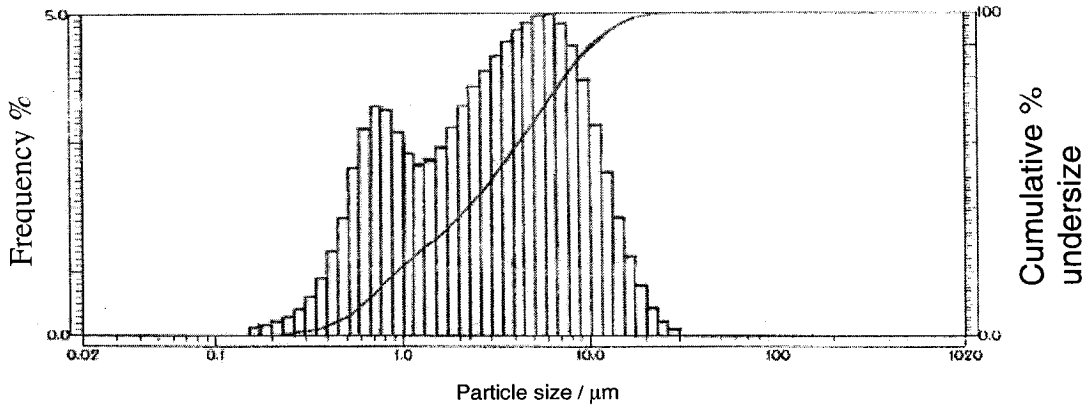

Figure 4.4. Particle distribution as received of HSC1200 (12 µm)

4.1.2 Pure magnesium and AZ91

The pure magnesium and magnesium alloy (AZ91D) used to infiltrate the composites was commercially pure grade. The chemical composition of magnesium-alloy (AZ91D) was given in *Table 4.2.*

Table 4.2. Composition of Magnesium alloy (AZ91D) (wt%)

Al	Mn (a)	Zn	Mg
9.0%	0.13%	0.7%	Balance

4.2 Composite Fabrication

4.2.1 Compact Preparation

Porous compacts of SiC particles were prepared for infiltration as shown schematically in *Figure 4.5.*

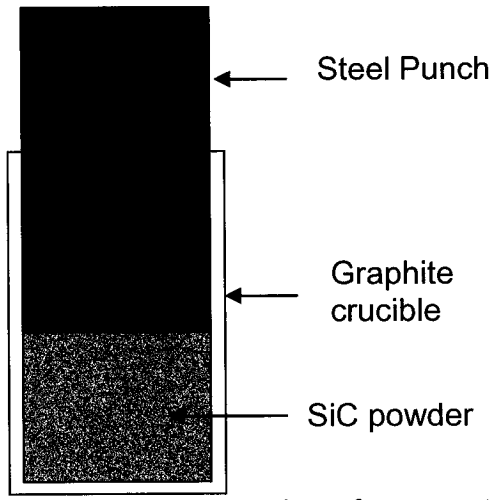

Figure 4.5 Schematic preparation of compaction

The dimension of graphite crucible was in 30mm I.D and 40mm O.D. About 25g of lose powder was poured into the crucible. Then a 0.5 kg steel punch with 30mm O.D was placed on the powder for 2 hours.

4.2.2 Infiltration Equipment

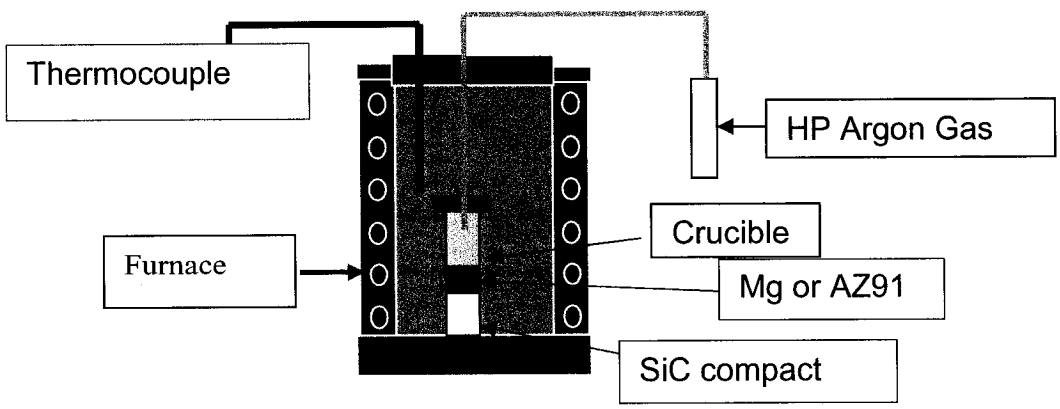

Figure. 4.6 Schematic diagram of experimental setup

The equipment consists of an electric furnace, a thermo-couple and protective gas station. The heating zone of the electric furnace is 120 mm in length. In order to prevent magnesium or magnesium alloy from oxidation at elevated temperature, high purity argon gas was employed in the chamber.

4.2.3 Infiltration Processing

After experimental equipment setup, the graphite crucible containing the SiC powder compact and amount of magnesium or AZ91 (15g) were carefully place in the furnace.

Infiltration was used to fabricate the composite materials. After melting, the magnesium gradually infiltrated the SiC compact. Experiments were performed at both 700°C and 800°C. The temperature curve is shown in *Fig.4.7*.

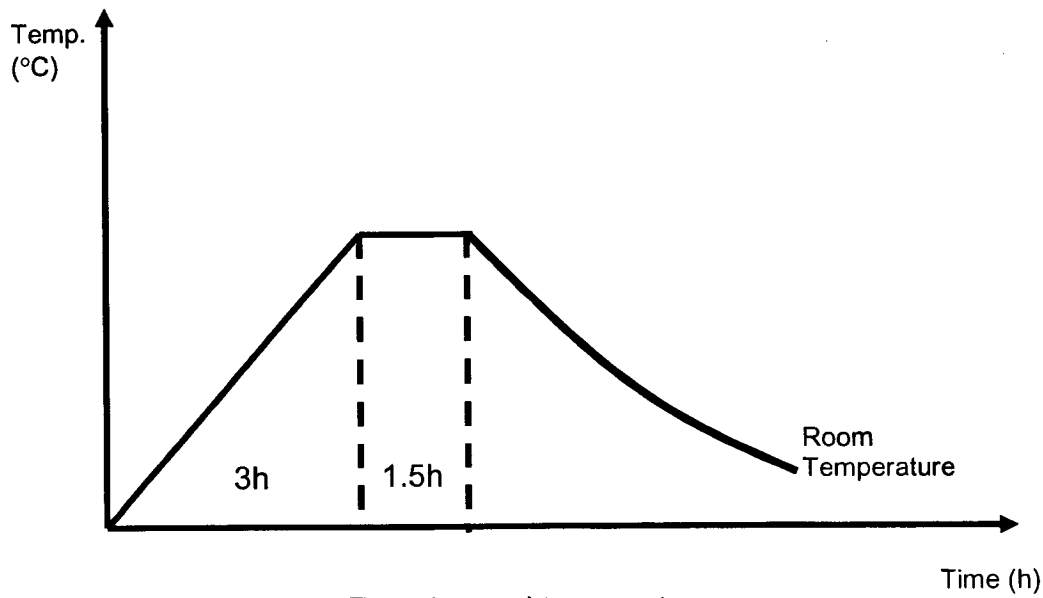

Figure 4.7 Experimental temperature curve

The heating rated was manually controlled at 3.5 – 4 °C /min., after the desire temperature was reached, the temperature was maintained for 90 minutes, and then furnace cooled to room temperature in order to enable easy removal of crucible.

4.3 Microstructural Characterization

4.3.1 Density and Porosity Determination

The bulk density of the infiltrated composites was determined using the Archimedes' principle as described in ASTM standard C20-97 [50]. The method involves first measuring the dry weight of the specimen (D). The specimen is then placed in water and boiled for 2 hours. After boiling, it is cooled while still completely immersed in water for a minimum of12 hours. The wet suspended mass in water (S) and the saturated mass in air (W) were measured. Knowing the density of pure water is equal to 1.0 g/cm^3 at 25 °C, the following equations are used to calculate the apparent porosity or open porosity (P) and the bulk density (ρ_B):

$$P\ (\%) = \frac{W-D}{V} = \frac{W-D}{W-S} \times 100 \qquad (4.1)$$

$$\rho_B = \frac{D}{V} = \frac{D}{W-S} \qquad (4.2)$$

4.3.2 Sample preparation for microanalysis

The sample sections were cut from the composite using a diamond blade. The polished surfaces were manually ground on 60, 120, 240, 400, and 600 grit SiC paper. Following this procedure, the samples were then automatically polished with a soft, long-napped, synthetic rayon cloth using 5 μm, 1 μm and 0.05 μm alumina polishing abrasive suspensions. The polishing was finished with 0.05 μm colloidal silica on a porous chemical-resistant synthetic pad.

4.3.3 Image analysis

In order to determine the content of SiC, optical image analysis was employed on polished sections. Image analysis functions on the differences in contrast between various phases in the system. The image analyzing system digitally processes optical images based on 256 gray level. The range of gray levels corresponding to the desired phase of interest (SiC) was digitally enhanced. An automatic stage pattern was set to compile similar data from each sample. Quantification of phases was achieved given that there was a detectable difference in contrast between the constituent phases.

4.3.4 Microscopy and Energy Dispersive Examination (EDS)

The microstructure of the composites is also examined by *JEOL JSM-840A* scanning electron microscope equipped with Energy Dispersive X-ray spectroscopy (EDS). Examination included reinforcement distribution, evaluation of porosity, cracks, metal/ceramic bonding, interface and matrix, reinforcement and interfacial region microanalysis.

The SEM was used either in the secondary electron (SEI) or backscatter electron (BSE) modes at 15 KeV. Due to the poor conductivity of SiC particulate, a thin gold-palladium coating was applied to the polished surfaces using an Anatech-Hummer VI sputter coater for imaging purposes in case of surface charging.

Secondary electron imaging (SEI) was used on samples to determine the distribution of SiC, porosity, crack and fracture surface. Backscattered electron imaging (BSE) provides contrast between chemically different phases in composites due to differences in atomic number.

Quantitative EDS analysis is performed on specific features within a sample on both polished and fractured samples. The X-ray mapping technique is performed to analyze the distribution of elements within polished samples.

4.3.5 X-Ray Diffraction (XRD)

In order to determine the crystalline phases in the composites, X-Ray Diffraction (XRD) was performed. The analysis was carried out on a Phillips APD-1700 X-Ray Diffractometer (CuK_α, 0.15406 nm), at an accelerating voltage of 40 KV and a beam current of 20 mA for angles 2θ of 0 to 130°.

4.4 Mechanical Testing

4.4.1 Hardness Testing

Hardness of bulk materials was performed with a standard Vickers Hardness Tester using a 10 kg load.

4.4.2 Shear Punch Testing [51,52]

The shear punch testing was essentially a blanking operation in which a punch is driven at a constant displacement rate, pushing the specimen down against the receiving die. It was instrumented to provide punch load-displacement data, which can be converted to tensile strength, ultimate tensile strength, and percent total elongation at fracture.

The general behavior of a specimen during shear punch testing is illustrated by the load-displacement curve as shown in *Figure 4.8*. The curve has features similar to a load displacement curve produced in a uniaxial tension test: an initial elastic region (P_t to P_y), followed by a departure from linearity at P_y, a non-linear increase in load with displacement, a maximum in load ($P_{max.}$) and a decreasing load with displacement to the point of failure.

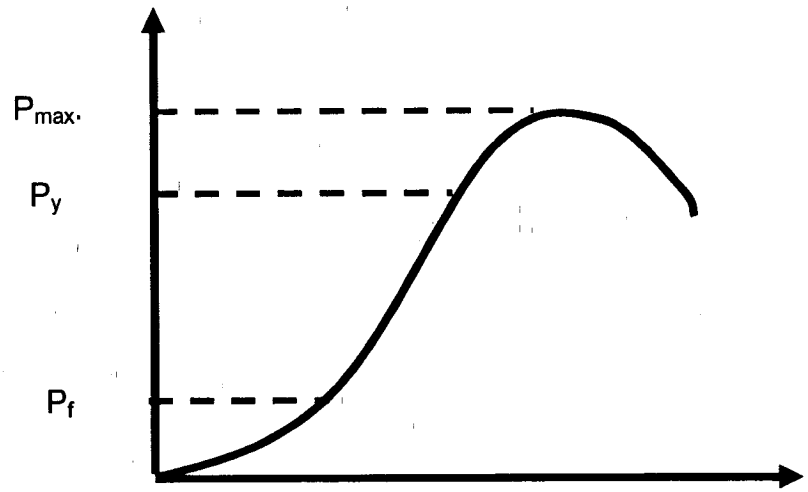

Figure. 4.8 The typical Load-displacement curve

It was found that the load at departure from linearity, Py, correlates well with the uniaxial yield strength and the load maximum, P_{max}, correlates well with the ultimate tensile strength, according to the empirical equation.

$$\sigma_{eff} = \frac{P - Pf}{2\pi r t} \qquad (4.3)$$

where,

P = either the yield or maximum load from the shear load displacement curve

σ = corresponding yield or maximum stress in tension

σ_{eff} = effective yield or ultimate stress in shear

P_f = friction load,

r = punch radius,

t = specimen thickness and C = correlation coefficient

P_f, P_y and Pm can be determined from the load-displacement curve as shown in *Figure. 4.9.*

In order to calibrate the shear punch data with standard tensile data, nine standard samples (copper:(3), brass:(3), and cold extruded copper: (3)) were measured before testing the composite samples.

Specimen sheets for shear punch testing were sliced into blanks of less 0.45mm in thickness using a diamond-wafering blade. The blanks were subsequently ground with SiC papers (120, 240, 400 and 600 grit). The final thickness of the blanks was less than 0.40mm.

MTS-810 hydraulic material testing system (as shown in *Figure. 4.9*) was used for shear punch testing using load cell of 25kN capacity.

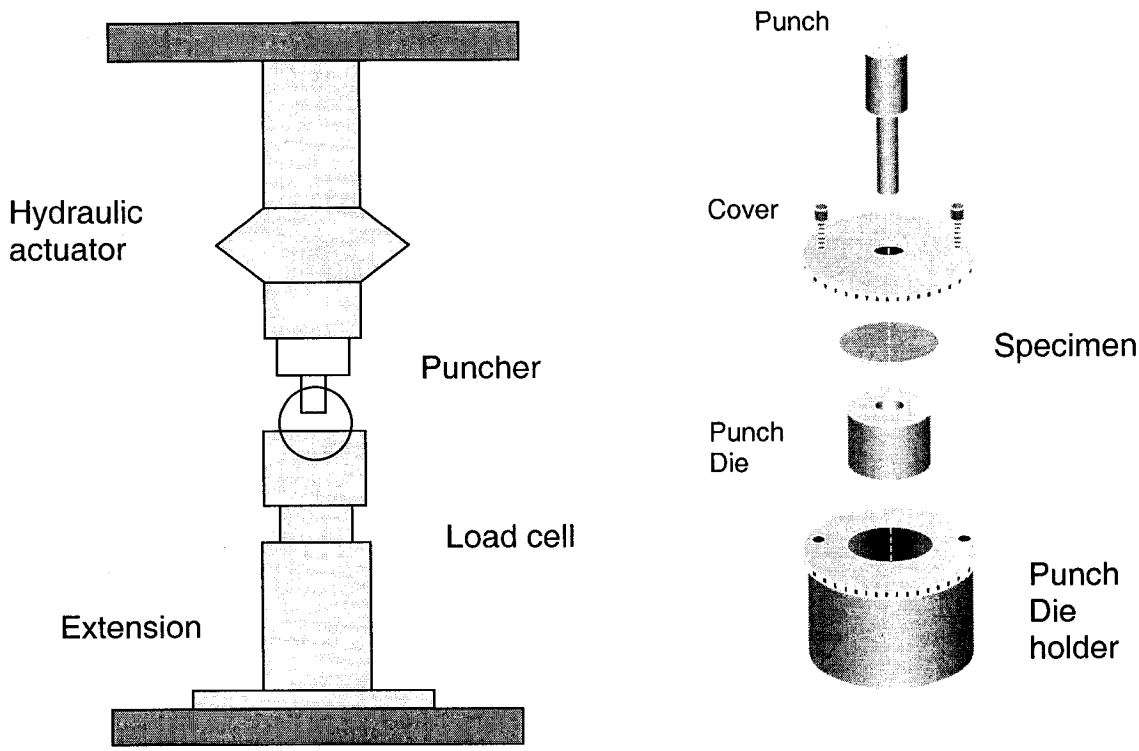

Figure.4.9 Schematic of shear punch test setup

MTS-810 hydraulic material testing system consists of an upper and lower housing, the upper housing contains a punch, and the lower one holds a die. The central axes of the punch and die are exactly aligned in the upper and lower housing. The sample is placed between the die and cover. The cover prevents the specimen from moving during load application. A flat tip punch is forced through the specimen, and the action of the punch against the die shears a circular dish from the specimen, completing the test.

In the present work, the diameter of the punch is 2.95mm, and a constant punch displacement rate of 0.667mm/min was used throughout.

Chapter 5

Results

5.1 Microstructure of SiC powders:

The starting powders were examined by Scanning Electron Microscopy (SEM) and the resulting micrographs are shown in *Figure. 5.1.*

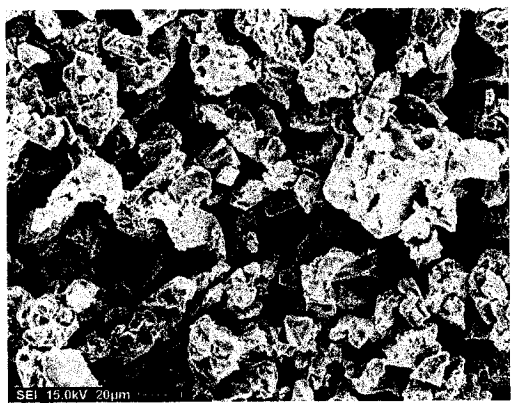

a)

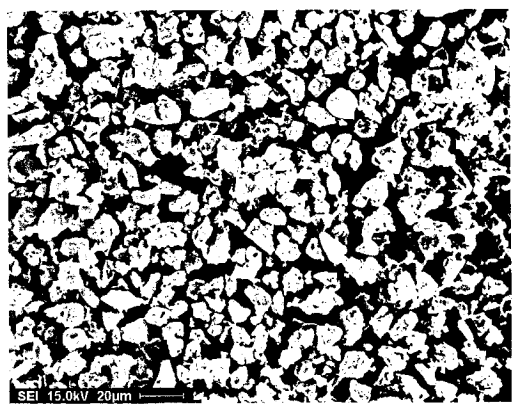

b)

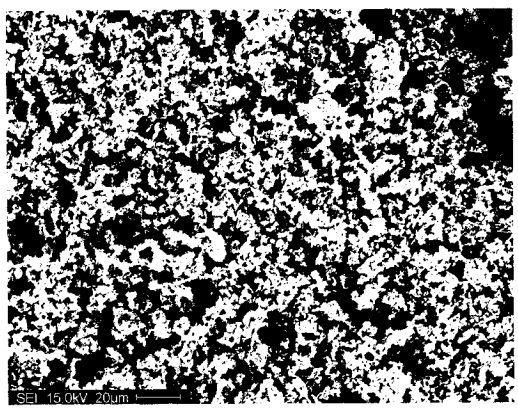

c)

Figure.5.1 The microstructure of as received SiC powder. a) 38µm, b) 22µm, c) 12µm.

The microstructure of starting SiC powder was granular shape and known to be covered by a thin layer of SiO_2 and some free silicon. At high magnification, Pores were observed as shown in *Figure 5.2.*

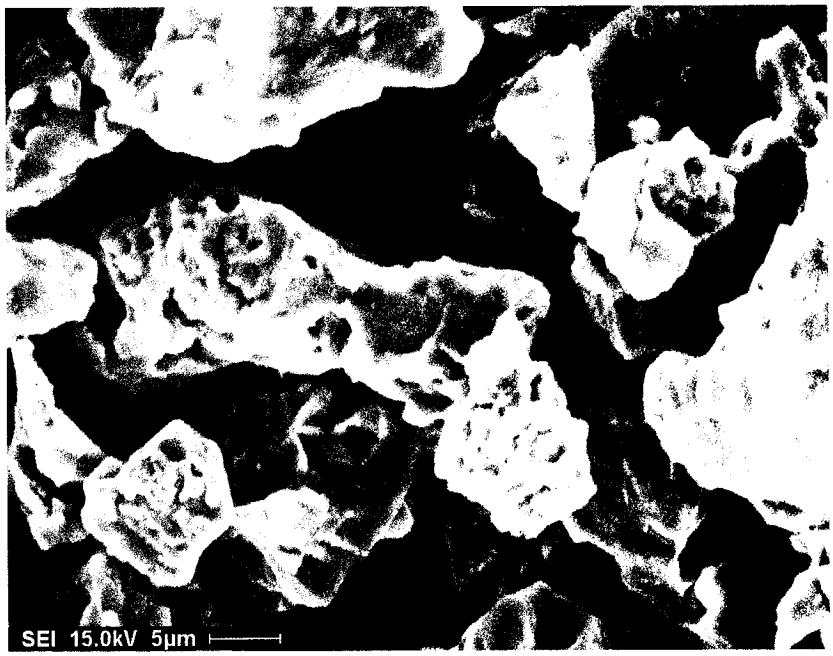

a)

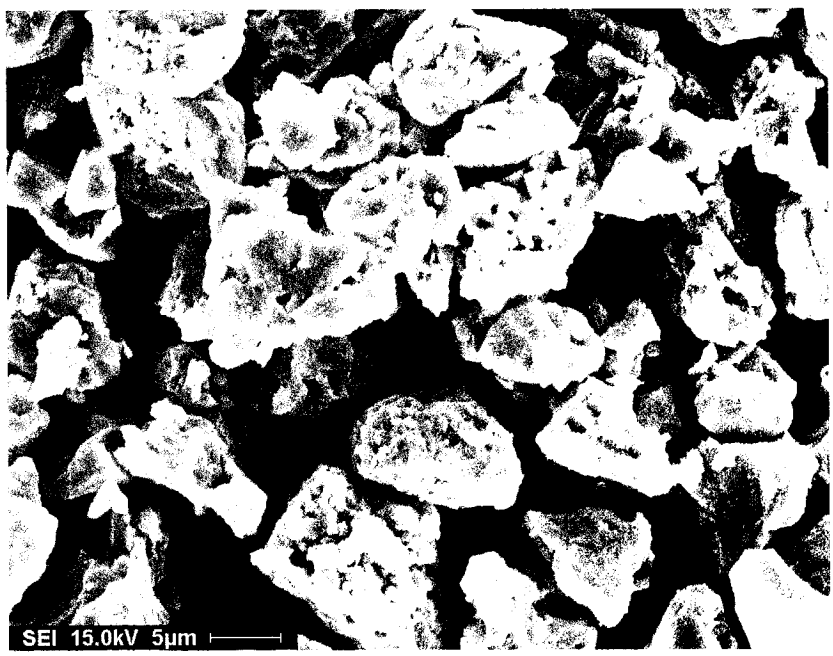

b)

Figure 5.2. The micropores presented in the body of the SiC powders (a) 38µm, b) 22µm.

The micro-pores exist in the body of SiC powders and result in an increase in surface area and surface energy of the SiC powder. The increase would affect the infiltration process.

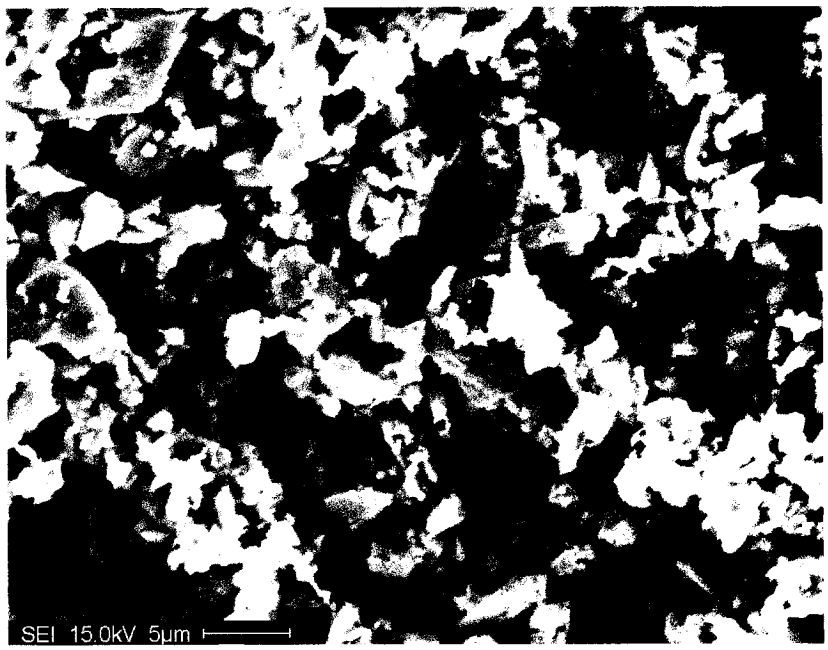

Figure 5.3 The microstructure of starting 12 µm SiC powder at high magnification

Figure 5.3 revealed that starting in 12 µm SiC powder, (i) the coarse powder was covered by finer particle; (ii) the finer particle was easily agglomerated.

5.2 Composites fabrication:

5.2.1 SiCp/Mg composites:

The infiltration experiments were successfully carried out at 700°C and 800°C. The microstructures of composites are shown in *Figure. 5.4* and *Figure. 5.5.*

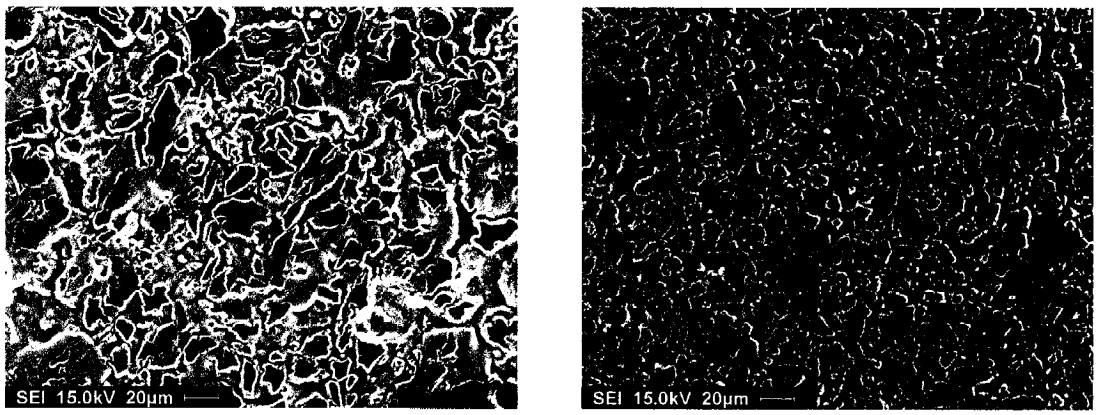

a) b)

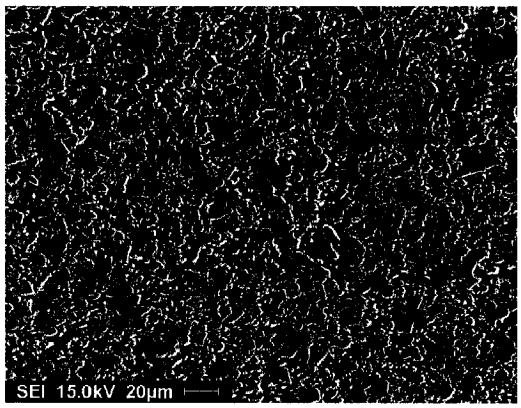

c)

Figure. 5.4 SEM micrographs of infiltrated samples at 700°C. a) 38µm, b) 22µm, c) 12µm.

The results of SEM studies conducted on the SiCp/Mg samples revealed that at either 700 °C or 800 °C (i) SiC was successfully incorporated into pure magnesium matrix; (ii) good uniform and even distribution of SiC powder occurred in the Mg matrix; (iii) SiC particulates are located in both intergranular and intragranular locations; (iv) the presence of porosity is minimal, as indicated in *Figure. 5.4* and *5.5.*

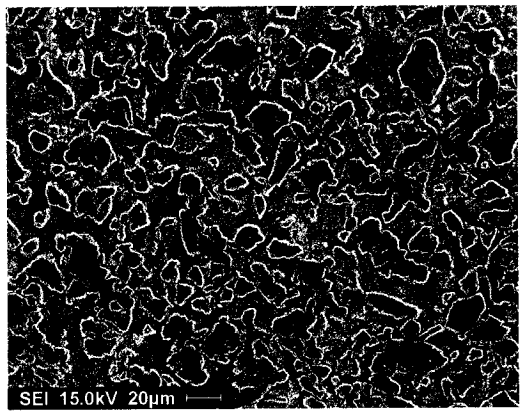

a)

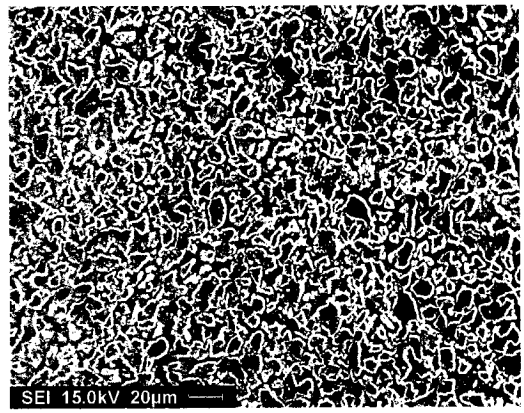

b)

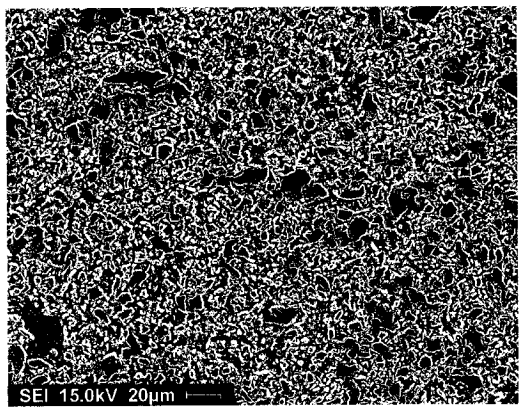

c)

Figure. 5.5 SEM micrographs of infiltrated samples at 800°C. a) 38µm, b) 22µm, c) 12µm.

However, at high magnification, the results of SEM studies conducted on SiCp/Mg samples show when the particle size of SiC is 38µm or 22µm, microcracks exist in the composites. On the other hand, when the particle size of SiC is 12µm, there is no apparent cracking in the composites as revealed in *Figure. 5.6* and *5.7.* In addition, when the particle size of SiC is 38µm or 22µm, there is porosity in the samples; when the particle size of SiC is 12µm, there is no apparent porosity in the samples.

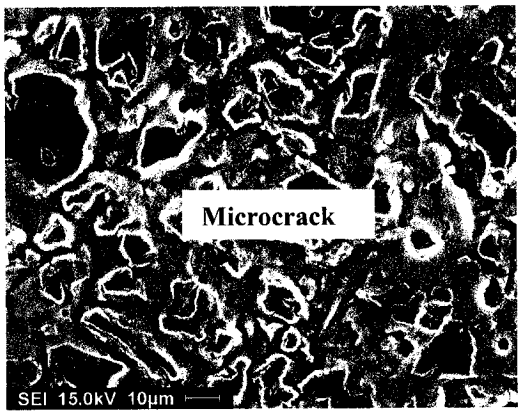

a)

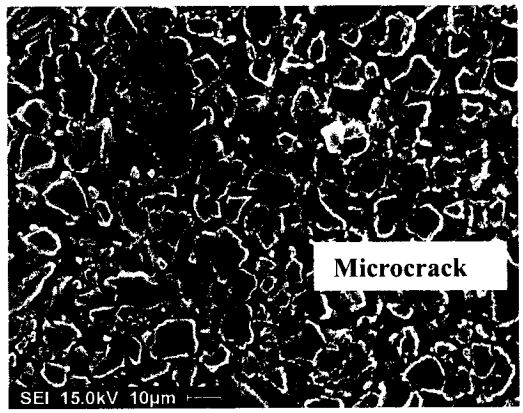

b)

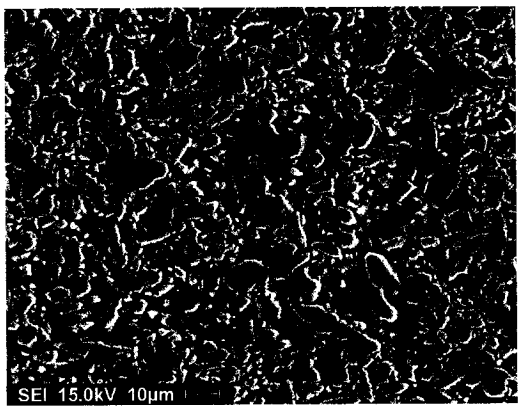

c)

Figure. 5.6 SEM micrographs of polished Mg/SiC composites infiltrated at 700ºC.Particle size of SiC is a) 38µm, b) 22µm, and c) 12µm.

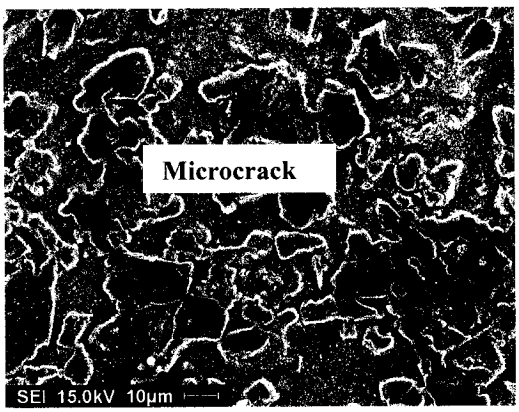

a)

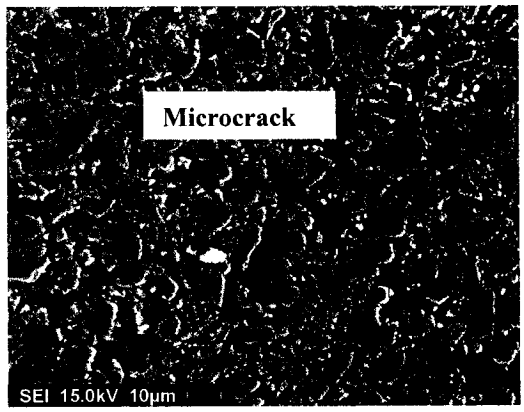

b)

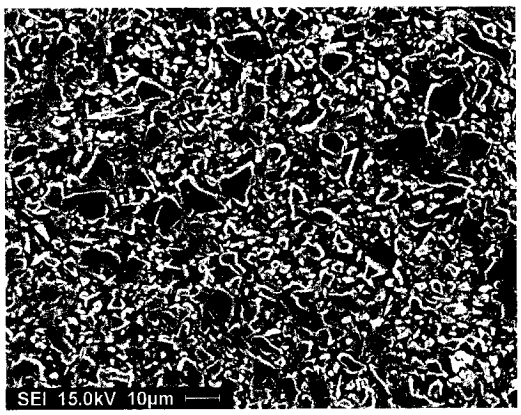

c)

Figure. 5.7 SEM micrographs of SiCp/Mg infiltrated at 800°C. Particle size of SiC is a) 38µm, b) 22µm. and c)12µm.

Comparison of the microstructures of composites at different infiltration temperature indicated that there was less porosity when processing at 800 °C than at 700 °C.

5.2.2 SiCp/AZ91 composites

The infiltration experiments were carried out at 700°C. The results of SEM studies at low magnification are shown in *Figure. 5.8.*

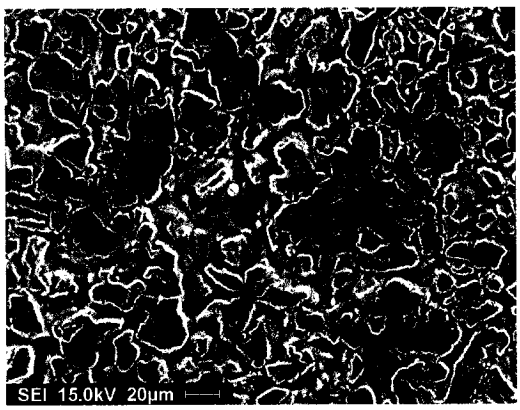

a)

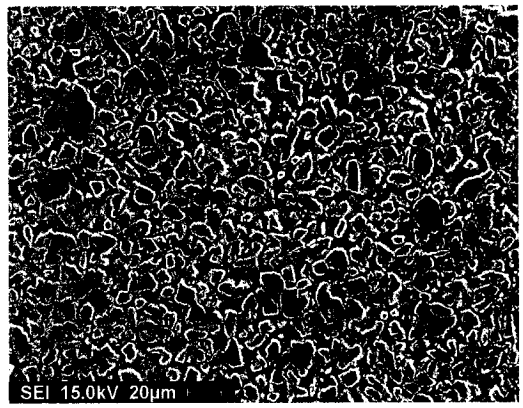

b)

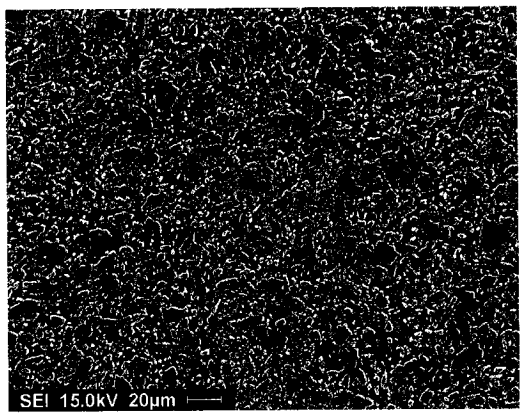

c)

Figure 5.8 SEM micrographs of AZ91/SiC_p samples infiltrated at 700°C.
a) 38µm, b) 22µm, c) 12µm.

The results of SEM studies conducted on the SiCp/Mg alloys samples reveal that at 700 °C (i) SiC is successfully incorporated into the AZ91 matrix; (ii) good uniform and even distribution of the SiC powder occurred in AZ91 matrix; (iii) SiC particulates are located in both the intergranular and intragranular locations.

Microstructures (Figure 5.9) show (i) when the particle size of SiC is 38µm or 22µm, microcracks exist in the composites; (ii) on the other hand, when the particle size of SiC is 12µm, there is no apparent cracking in composites

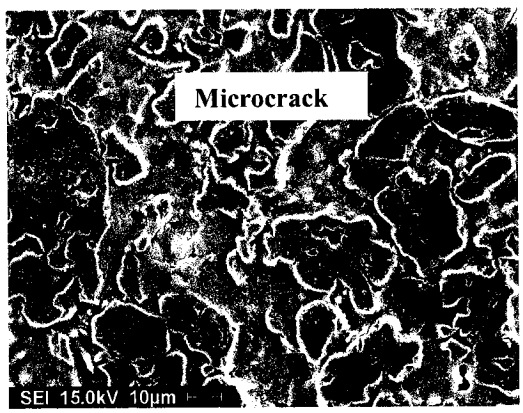

a)

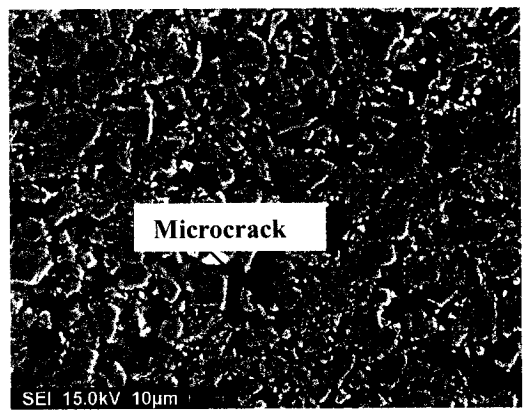

b)

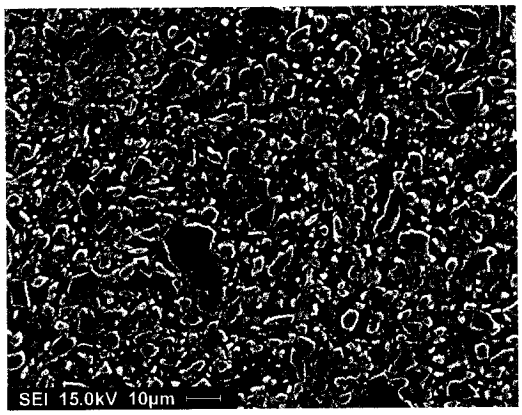

c)

Figure 5.9 SEM micrographs of AZ91/SiC_p infiltrated at 700°C at high magnification. The particle size of SiC is a) 38μm, b) 22μm, and 12μm.

5.3 Density and porosity

The results of density and porosity measurements were conducted using Archimedes method. The results were shown in *Table 5.1.*

Table 5.1 Density and porosity under various processing conditions

	Infiltration temp. (°C)	Particle size of SiC (μm)	Density (g/cm^3)	Open Porosity (%)
Mg/SiC_p	700	38	2.28	2.45
		22	2.41	1
		12	2.53	0
Mg/SiC_p	800	38	2.19	1.9
		22	2.36	0.5
		12	2.51	0
AZ91/SiC_p	700	38	2.31	1
		22	2.41	0.6
		12	2.55	0.6

The results reveal that (i) the density of these composites increases with the decrease of particle size of SiC; (ii) the porosity increases with increase of

particle size, and, decreases with the increase in infiltration temperature; (iii) the infiltration temperature has minor effect on density.

5.4 SiC volume fraction measurement

Measurement of SiC content was performed using optical image analysis. The average SiC content in the various samples are listed in *Table 5.2.*

Table 5.2 SiC content as measured by optical image analysis

	Infiltration temp. (°C)	Particle size of SiC (μm)	SiC content (Vol.%)
Mg/SiCp	700	38	15.5
		22	16.7
		12	33.3
Mg/SiCp	800	38	15.6
		22	16.7
		12	33.5
AZ91/SiCp	700	38	15.4
		22	16.6
		12	33.7

5.5 Matrix and Ceramic Interaction

Figure. 5.10 shows a representative interfacial region of the Mg/SiC_p composite. The micrograph of interfacial region revealed a clean featureless interface between the matrix and reinforcement.

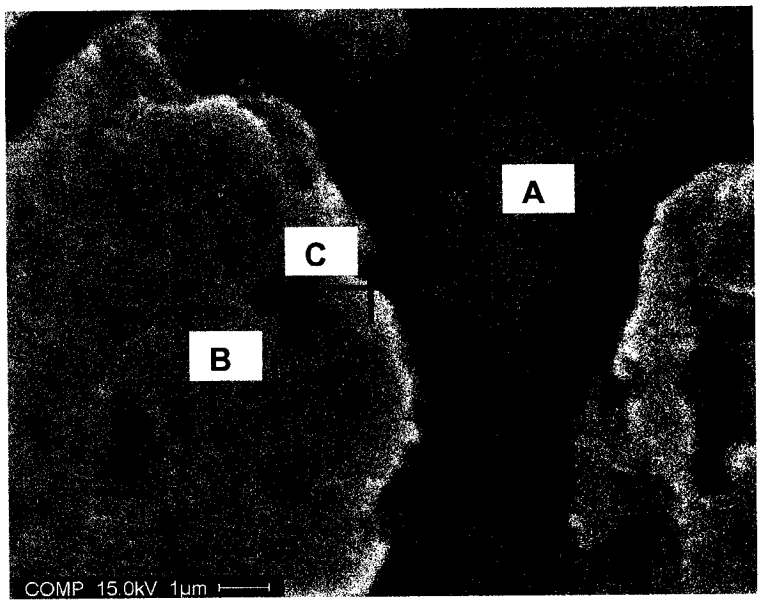

Figure. 5.10 Typical interfacial region of Mg/SiC (22µm) composite (700°C)

The results of EDS analysis conducted on the composites at the different locations on the *Figure. 5.10* reveal that (i) at "A" point, the main elements is Mg (see *Figure. 5.11* a)); at "B" point, the elements are Si and C (see *Figure. 5.11 b*)); (iii) at "C" point, the main elements detected are Mg, Si, O and C (see *Figure. 5.11* c))

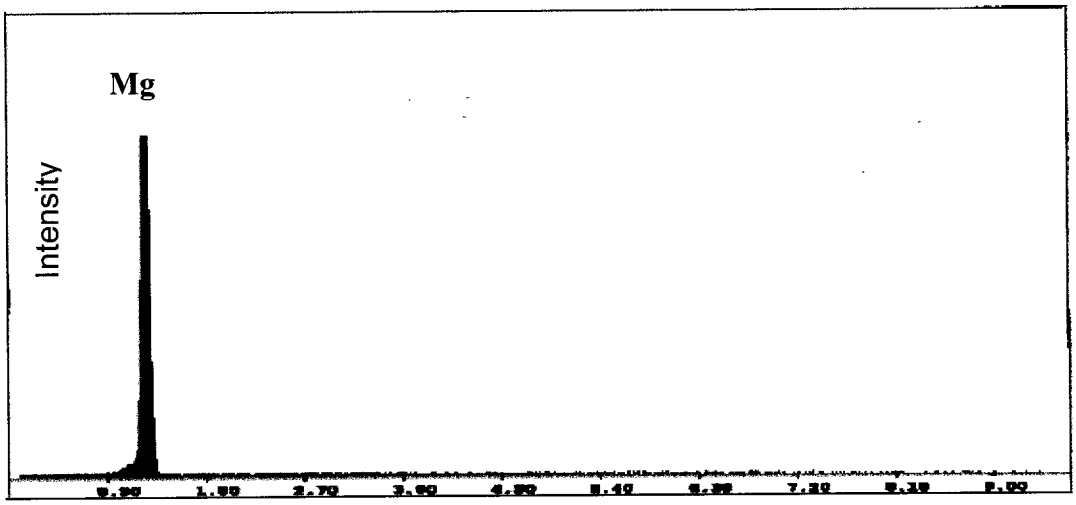

a)

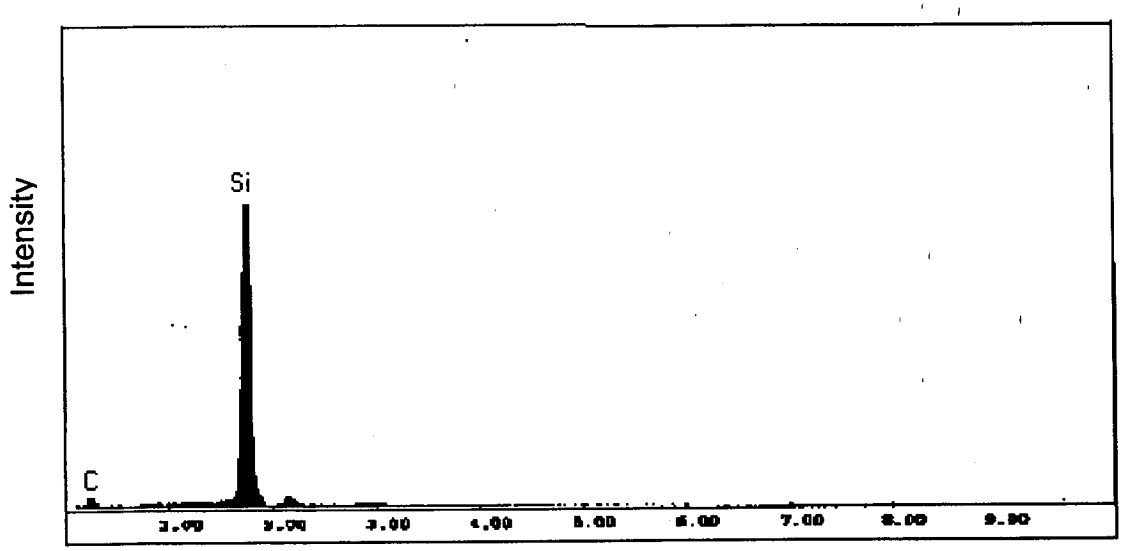

b)

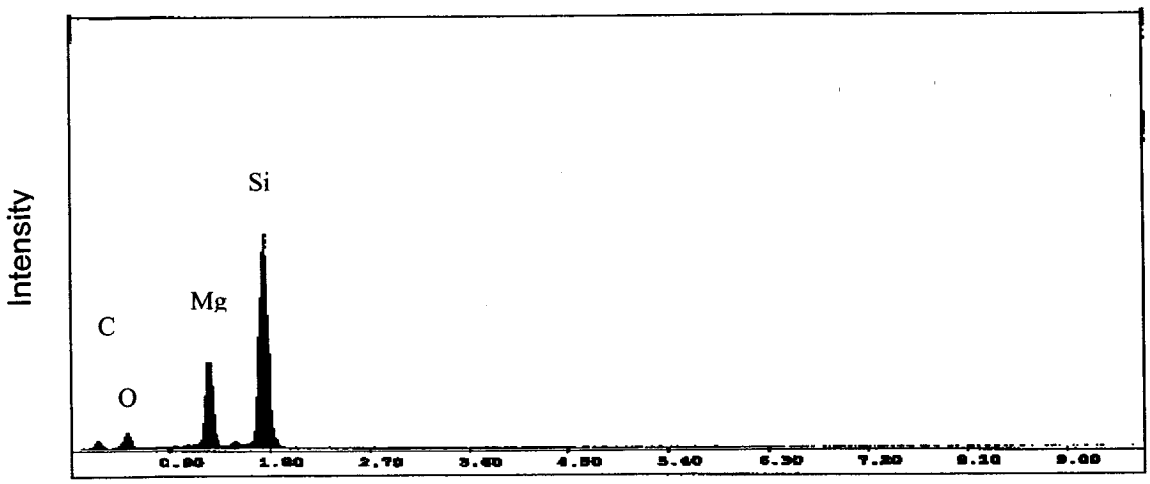

c)

Figure. 5.11 EDS spectra for different positions at Mg/SiC interface in Mg/SiC composites. A) Matrix, b) SiC powder, c) Mg-SiC interface.

The results of XRD revealed that crystalline Mg, SiC, Mg_2Si and MgO were presented in the composites. However, the amount of Mg_2Si and MgO is < 5%.

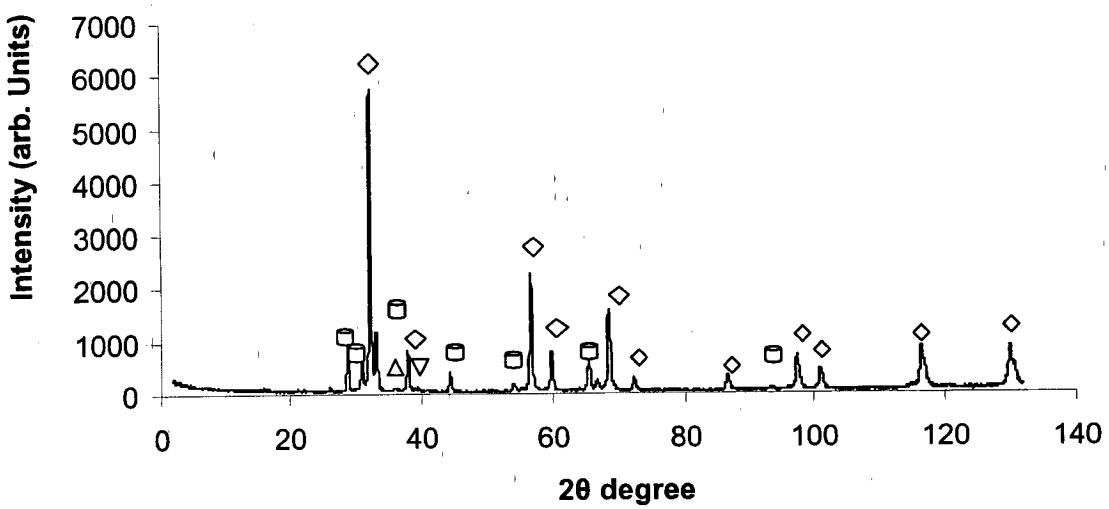

a)

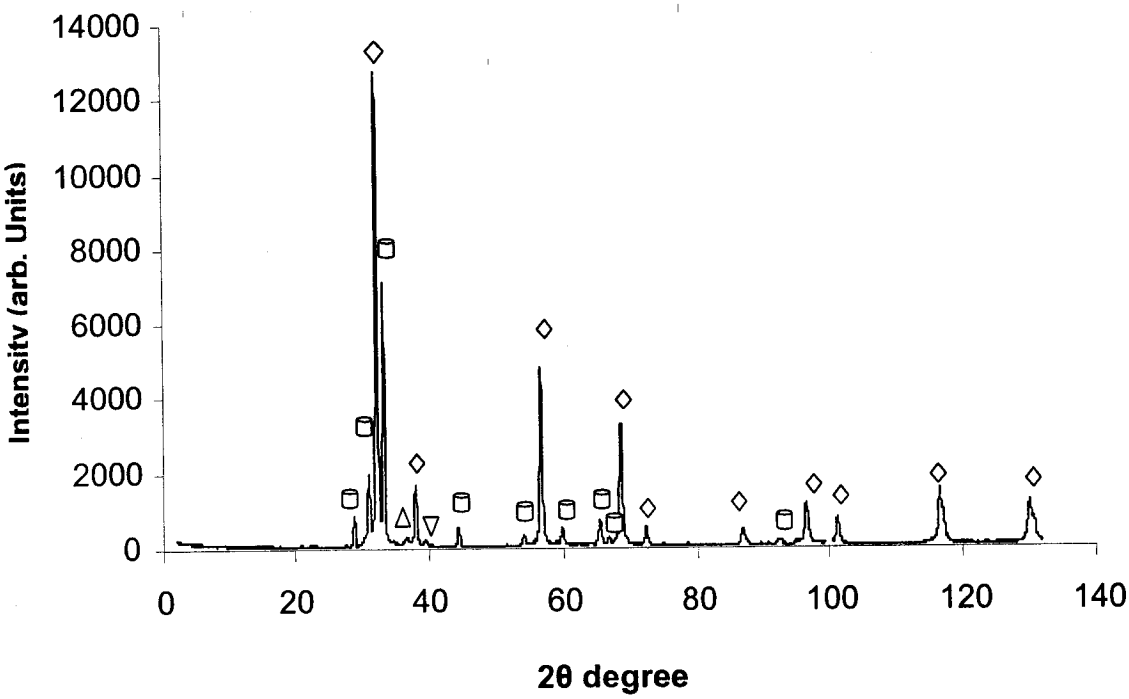

b)

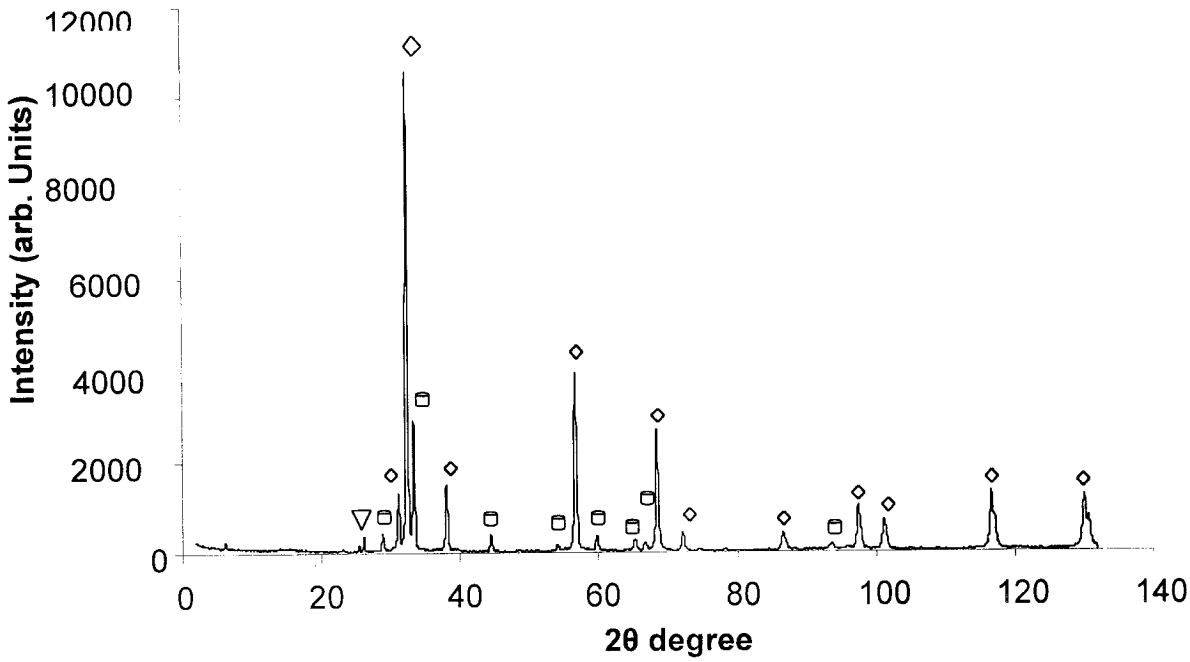

c)

Figure.5.12 XRD spectra of Mg/SiC composites with different particle size of SiC reinforced. a)12 μm, b) 22 μm, c) 38 μm.
SiC - ◇ Mg - ⛁ Mg_2Si - △ MgO - ▽

5.6 Mechanical properties

5.6.1 Hardness

The results of hardness measurement are shown in *Table 5.3.*

Table 5.3. Hardness at various conditions

	Infiltration temp. (°C)	Particle size of SiC (μm)	Hardness (HV_{10})
Mg/SiCp	700	38	108
		22	196
		12	265
Mg/SiCp	800	38	70.2
		22	193
		12	232
AZ91/SiCp	700	38	160
		22	198
		12	302

The results revealed that (i) the hardness of composites increased with the decrease of particle size of SiC, i.e. with increase of volume fraction of SiC; (ii) comparison of the Mg/SiCp composites at different infiltration temperature, showed that the hardness was higher at 700 °C than that of at 800 °C considering the same particle size; (iii) comparison of the Mg/SiCp and AZ91/SiCp composites, the hardness of AZ91/SiCp was higher than that of Mg/SiCp for the same particle size of SiC.

5.6.2 Shear properties

A typical load-displacement curve is shown in *Figure.5.13*. The curve is similar to a load-displacement curve produced in a uniaxial tension test: an initial linear region, followed by a departure from linearity, a non-linear increase in load with displacement, a maximum in the load, and a decreasing load with displacement to the point of failure.

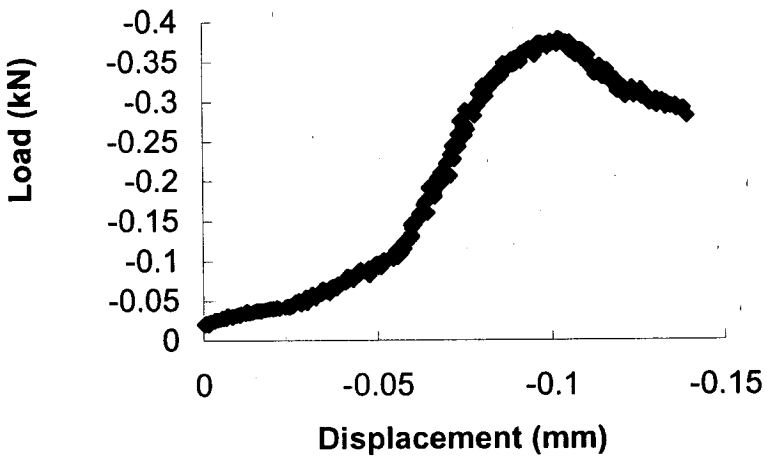

Figure.5.13 Typical load-displacement curve of a shear punch test of Mg/SiC (38 μm) at infiltration temperature: 700˚C.

5.6.2.1 Displacement at fracture to thickness ratio (D_f/t)

From load-displacement curve, it was possible to predict the elongation by applying displacement at fracture to thickness ratio (D_f/t) [53, 54]. The average of D_f/t at various composites is shown in *Table 5.4.*

Table 5.4 Average of D_f/t at various composites measurement

	Infiltration temp. (˚C)	Particle size of SiC (μm)	D_f/t (%)
Mg/SiC_p	700	38	22.56
		22	15.72
		12	13.25
Mg/SiC_p	800	38	22.33
		22	15.46
		12	12.33
$AZ91/SiC_p$	700	38	18.50
		22	13.56
		12	10.36

The result of elongation measurement showed that (i) elongation decreases with increase in volume fraction of SiC; (ii) processing temperature has no apparent effect on elongation in the composites.

5.6.2.2 Tensile strength

i) Effect of SIC volume fraction on strength

By maintaining a constant specimen thickness, the shear load-displacement behavior of the various particle size SiC reinforced composites can be compared to some extent. For the composite tested, the load-displacement curves appear to correspond with the tensile results (*Figure.5.14*)

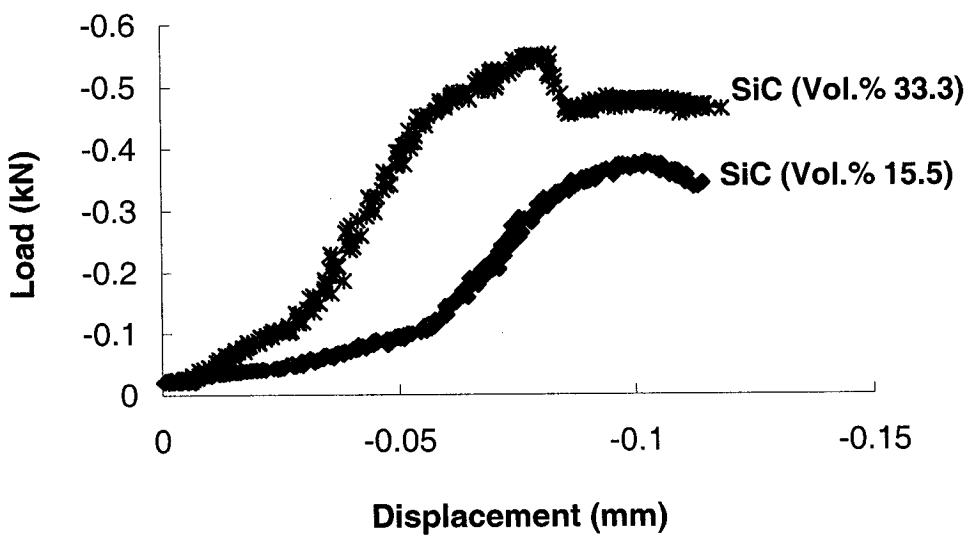

Figure. 5.14 Load-displacement curves of Mg/SiC_p composites at different particle size (Mg/SiC composites were prepared at 700 °C)

The load-displacement curves reveal that (i) the load increases with increase of SiC content; (ii) for the composite reinforced with less SiC content, load transfer became difficult.

3.2 Effects of different infiltration temperature

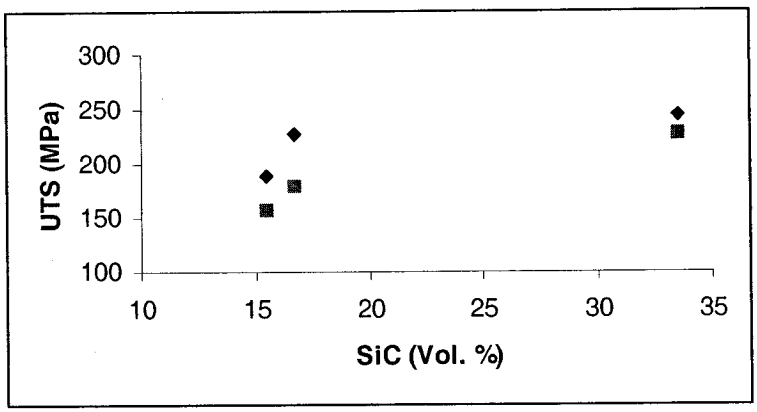

Figure.5.15 Relationship between the infiltration temperature and UTS.
■ - 800 °C, ◆ - 700 °C.

Figure.5.15 showed that (i) when the infiltration temperature was 700 °C, the strength increased with volume fraction of SiC and finally reached a plateau (ii) when the infiltration temperature is 800 °C, the strength increased with increase of volume fraction of SiC also the gradient increases; (iii) the strength of composites produced at an infiltration temperature of 700 °C is higher than that of 800 °C.

3.3 Effects of matrix

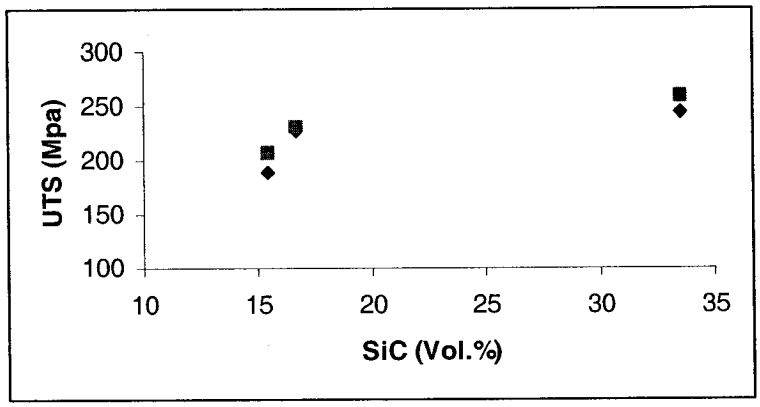

Figure. 5.16 Relationship between matrix and composites strength
■ - magnesium alloy (AZ91) ◆ - pure magnesium

Figure. 5.16 showed that the UTS of AZ91/SiC_p composite is slightly (5-10%) higher than that of Mg/SiC composite reinforced with same volume fraction of SIC particulate.

Chapter 6

Discussion

6.1 Synthesis SiC_p/Mg composites:

Both the pure Mg and Mg alloy (AZ91) successfully infiltrated into the different SiC perform at 700 ° C and 800 °C (see *Figure 5.4, 5.5* and *5.8*). No external pressure was applied to molten Mg or AZ91 and the infiltration processes were spontaneous.

The spontaneous infiltration strongly depends on the capillary pressure created by a porous preform. The capillary pressure drop equation is given as

$$\Delta P_\gamma = -\gamma S\cos\theta \qquad (6.1)$$

where γ is the surface tension of the melt, θ is the contact angle, and S is the specific surface area of the reinforcing phase. ΔP_γ is the pressure drop that drives the flow of the molten metal through the porous preform. When ΔP_γ is negative, the infiltration is spontaneous; when ΔP_γ is positive, there is no infiltration [53].

In the case of SiCp/Mg composites, Kaneda and Choh [23] studied the spontaneous infiltration process in magnesium composite fabrication. In their experiments, the fine SiO_2 covered the surface of coarser SiC powder. Mg reacted with Si or SiO_2 at 750 °C to form Mg_2Si. From Mg-Si binary phase diagram shown in *Figure 6.1* [11]. It can be seen that the melting point of Mg_2Si is around 1100 °C and much higher than the experimental temperature. As a result of the reaction, Mg_2Si precipitated on the SiC particles, increasing the wettability between Mg and the ceramic. It was believed that the contact angle between Mg and SiO_2 is less or equal to 90° and hence wetting occurs. Considering the as received SiC is always covered with a thin layer of SiO_2, it is reasonable to assume that the contact angle between Mg and SiC is low and wetting occurs. This would result in ΔP_Y

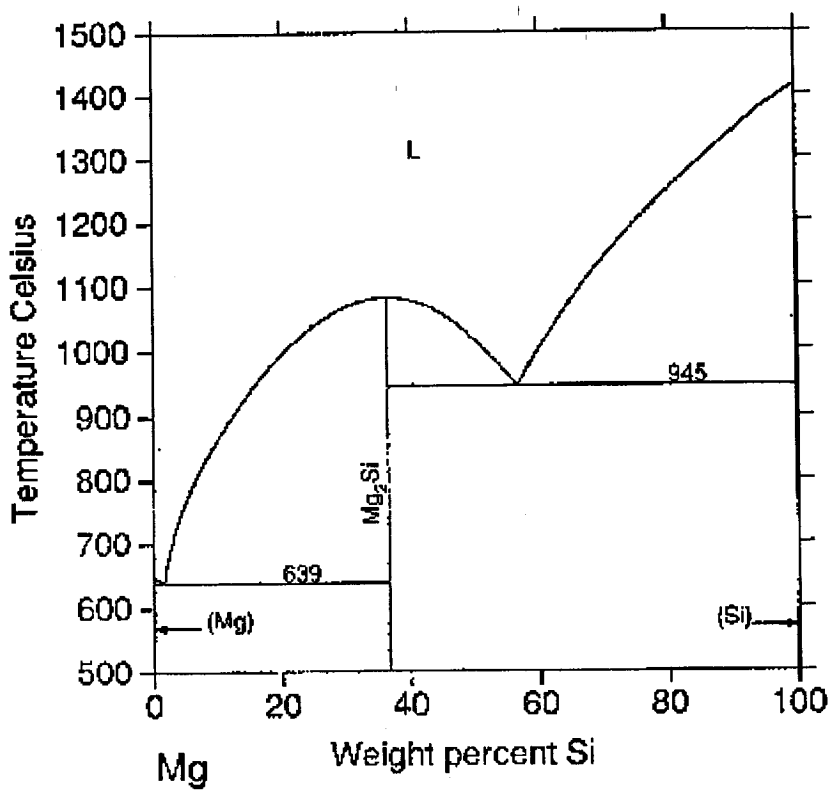

Figure 6.1 Mg-Si binary phase diagram

This would result in ΔP_γ being negative and so the infiltration process would be spontaneous as observed.

From the powder characteristics provided by manufacture, the specific surface area of SiC increased with decrease of particle size. Meanwhile, the average surface tension of pure Mg is constant at the present experimental temperature [11]. The proposed correlation between ΔP_γ and particle size of SiC is plotted as *Figure 6.2*.

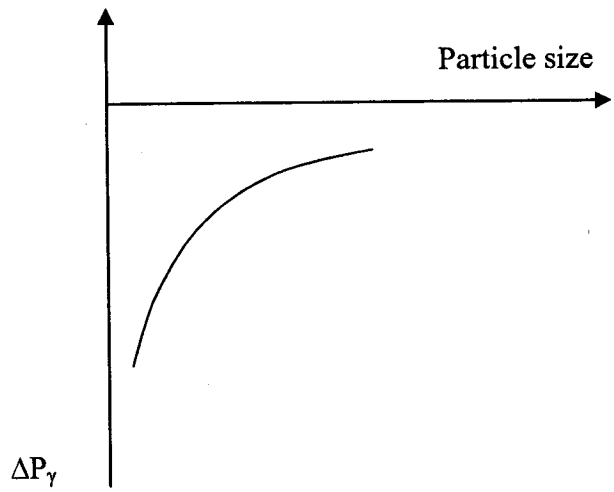

Figure 6.2 Correlation between ΔP_γ and particle size

The curve indicates that the driving force increases with decrease of particle size and this is consistent with experimental findings.

6.2 Porosity

The porosity measurement (see *Table 5.1*) indicates that porosity exists in the composites and is created for the following reasons [54]:

- insufficient infiltration of the reinforcement by the matrix,
- gas inclusions which may form within the composites during the infiltration of the reinforcement, and
- shrinkage due to superheating followed by solidification of the liquid metal.

It is difficult to estimate the amount of gas inclusions within the composites. The gas inclusion quantity in the composites depends on the direction of metal flow during infiltration and the process of matrix solidification. When the reinforcement is filled from below, there are good conditions for removing the gas from the casting and possible inclusions are moved to the raiser head through the solidification front [54].

The filling of capillary spaces in the reinforcement proceeds with the principle of minimum resistance, i.e. first the largest capillaries are filled and then as time passes, smaller and smaller capillaries get filled. In the process, it is very probable that gas gets entrapped. Two probable sources of gas are moisture, absorbed on the particle surface, and atmospheric bubbles entrapped in the particle aggregates. Magnesium reacts with moisture to form dissolved hydrogen. The local oversaturation of liquid metal in hydrogen may result in the nucleation and growth of gas bubbles.

In the present study, *Table 5.1* reveals that the open porosity decreases with increase of SiC content. This is attributed to the infiltration process. With coarser particles, the interparticle spacing is larger. As mentioned earlier, the molten Mg easily infiltrates into the larger channels after short times. Therefore, the gas is entrapped in smaller channels and micro-pores (*see Figure 5.2*), resulting in no infiltration at gas oversaturation areas and results in porosity formation. On the

other hand, with fine particle, the infiltration is more homogeneous, the gas at the surface of SiC easily escapes, resulting in little or no porosity.

6.3 Interfacial reaction

Interfaces play an important role in achieving strengthening in a composite. The ability to improve strength is dependent on the ability to transfer stress from the matrix to the high strength-reinforcing particles. This, in turn, is dependent on achieving a strong interfacial bond between the matrix and reinforcement. If the interfacial bond is weak, the interface would fail before any effective stress transfer to the particle, and no strengthening would be achieved. The composite may, in fact, appear to be weaker than the uninforced matrix because of the reduced effective area supporting the load [4]. Due to the high reactivity of magnesium, the interfacial microstructure between magnesium and reinforcements has attracted a great deal of attention in recent research. The nature of the interface in SiC reinforced Mg matrix composites is discussed in this section.

Magnesium does not form a stable carbide and the SiC reinforcement, therefore, SiC is thermodynamically stable in liquid magnesium. The most common type of interfacial structure observed consists of an essentially featureless interface in which matrix and eutectic are in intimate contact with particles. There was no evidence of extensive chemical reaction at the interface [39].

However, since a small amount of free silicon and silica exists on the surface of the reinforcement [20], magnesium reacts with these compounds, observed in *Figure 5.12*. The probable reactions are as following:

$$4Mg + SiO_2 = Mg_2Si + 2\,MgO \qquad (6.2)$$

$$\Delta G_1 = -338.6\ kJ \qquad (700\ ^\circ C)$$

$$2Mg + Si = Mg_2Si \qquad (6.3)$$

$$\Delta G_2 = -140\ kJ \qquad (700\ ^\circ C)$$

Considering the experimental procedure, SiC particulates also absorb oxygen on the surface. Magnesium reacts with O_2 to form MgO:

$$2Mg + O_2 = 2MgO \qquad (6.4)$$

$$\Delta G_3 = -1051\ kJ \qquad (700\ ^\circ C)$$

In order to identify these reactions, microanalysis by EDS and X-Ray Diffraction (XRD) were employed. The results verify these reactions within the SiC/Mg interface. The EDS spectra (*Fig.5.11*) show that the main elements present are Mg, Si, C and O. The XRD spectra show small peaks of Mg_2Si and MgO corresponding with EDS results and confirming the above reactions. Similar results were reported by Braszczynska and Bochenek using XRD and TEM techniques [36].

Also, the F*A*C*T thermodynamic analysis program confirms the possibility of the above reactions.

These reactions have an important effect on spontaneous infiltration process. Kaneda and Choh [23] investigated the effect of chemical reaction on the infiltration process. The results showed that the Mg-SiO_2 thermite reaction (equation 6.2) heats the infiltration front, and, silicon from reduced SiO_2, dissolves in the Mg melt and the melt becomes an Mg-Si alloy. Therefore, the Mg- SiO_2 thermite reaction is more important due to improved wettability occurring at higher temperature.

6.4 Mechanical Behavior

The mechanical properties in general associate with several factors, such as the distribution of reinforcement, volume fraction of reinforcement, type of matrix and reinforcement, interfacial reaction and fabrication technique. The reinforcement plays a predominantly important role in the mechanical properties of metal matrix composites.

6.4.1 Hardness

The results of hardness measurement revealed that an increase in volume fraction of SiC leads to an increase in the hardness. This can be attributed to (i) increasing the amount of harder SiC particulates in the matrix; (ii) higher SiC volume fraction resulting in a refined matrix microstructure: (iii) good bonding between matrix and reinforcement; (iv) high residual stress in the composites due to the difference of the coefficient of thermal expansion between the matrix and reinforcement.

Also, comparing the hardness of composites produced with different experimental conditions, the result reveals that there is no effect of infiltration

temperature on hardness. This is attributed to the hardness of composites being largely dependant on the volume of reinforcement. In addition, increasing the hardness of matrix, the overall (bulk) hardness will also increase.

6.4.2 Tensile properties

6.4.2.1 Deformation behavior of Mg/SiC composite during shear punch testing

A typical load-displacement curve of a shear punch test of Mg/SiC composite is shown in *Fig. 5.13*. As can be seen, the curve has features similar to a load displacement curve produced in a uniaxial tension compression test: that is, an initial linear region, followed by a departure from linearity, a non-linear increase in load with displacement, a maximum in load, and a decreasing load with displacement to the point of failure. This curve relates to the work hardening process of Mg/SiC_p composites.

Previous research [51, 52] investigated the different composites and materials deformation behavior during shear punch testing. It indicates that, for all materials tested, the point of initial departure from linearity corresponds to permanent penetration of the punch into the specimen. Between initial penetration and maximum load, the material work hardens sufficiently to compensate for thinning of the specimen in the process zone. At the maximum load, however, a point of plastic instability is reached, and subsequent deformation occurs under falling load conditions.

6.4.2.2 Effects of volume fraction on work hardening

Figure 5.14 shows the stress- strain curves for SiC_p/Mg, for two SiC volume fractions. The apparent working hardening rate is higher at low stains, and also

increases with decreasing SiC particle size. This is consistent with the observation made by Lloyd [4].

6.4.2.3 Ultimate tensile strength

Figure 5.15 shows that the ultimate tensile strength increased with decrease of SiC particle size. This can be attributed to the increase of dislocation density. Arsenault and Shi [55] used a model based on dislocation density to account for the strengthening ($\Delta\delta$) in the metal matrix composite reinforced with particulate. $\Delta\delta$ can be expressed as:

$$\Delta\delta = \gamma\mu b\rho^{1/2} \qquad (6.5)$$

Where γ is a constant of order of 1, μ is the shear modulus of the matrix, b is the Burgers vector of the matrix metal, ρ is the average dislocation density generated by the CTE mismatch.

In the present work, Owing to the large difference of coefficient of thermal expansion (CTE) between SiC and magnesium, the mismatch strain would result in an increase of dislocation density at the interface between SiC and magnesium after solidification. Dislocation density increased with decrease in particle size of reinforcement [4] i.e. an increase of the volume fraction of reinforcement. Therefore, the ultimate strength increased. However, it should be noted that when the infiltration temperature was 700 °C, a plateau was observed. This probably reflected difficulties in obtaining a uniform particle distribution at high volume fractions [4]. It suggested that a critical volume fraction exists in strengthening these Mg/SiC_p composites.

6.4.2.4 Effects of alloying elements (Al and Zn) on UTS

Fig. 5.16 shows that the UTS of composite with AZ91 matrix is 5-10% higher than that of composite with the pure magnesium matrix. This is in agreement with the continuum shear lag model. The model suggested that the composite strength is a parabolic function of the strength of matrix [4].

Comparison of pure magnesium and AZ91, the strength and hardness of AZ91 are improved by alloying elements, Al and Zn. Cai et al. [34] investigated the solidification process of a SiC_p/AZ91 composite. The results showed that the SiC particle was able to act as the substrate for the heterogeneous nucleation of the primary magnesium phase, and $Mg_{17}Al_{12}$ precipitates during solidification. As a result of precipitation, the strength and hardness of composites would be improved.

Chapter 7

Conclusions

1) SiC particulates were successfully incorporated into both pure magnesium and a magnesium alloy (AZ91) by applying a spontaneous infiltration technique. The particle size of SiC used were 38 μm, 22 μm and 12 μm. The infiltration temperature was 700 °C and 800 °C. High purity argon gas effectively prevents magnesium from oxidation at high temperature during processing.

2) A fairly uniform distribution of SiC particulates is achieved and only few pores and microsegregation were observed in the present study.

3) The infiltration process relates to the infiltration temperature, particle size of SiC and matrix. Increasing the infiltration temperature, decreasing the particle size of SiC results in more successful infiltration.

4) The microstructural analysis shows that microsegregation exists in composites when the particle size of reinforcement was 38 μm and 22 μm, however, on the other hand, when the particle size of reinforcement is 12 μm, the microsegregation was eliminated.

5) Microanalysis and X-Ray Diffraction (XRD) results verify reactions at the SiC/Mg interface as follows:

$$4Mg + SiO_2 = Mg_2Si + 2\ MgO$$

$$2Mg + Si = Mg_2Si$$

6) Typical load-displacement curves of shear punch tests of Mg/SiC composite has features similar to a load displacement curve produced in a uniaxial tension test.

7) Hardness of the composites increased with the decrease of particle size of SiC, i.e. increase of the volume fraction of SiC.

8) Strength (UTS) of composites increased with the decrease of particle size of SiC, i.e. increase in the volume fraction of SiC.

Recommendation for future work

Although the spontaneous infiltration process was achieved, future research must be directed at investigating the effects of the various parameters (infiltration temperature, infiltration time, particle size, etc.) on infiltration process and tailoring the process parameters. In order to accomplish this goal, larger scale experiments should be conducted.

The wettability between Mg and SiC is still uncertain. Additional work, focusing on the measurement of wettability would shed some light on what is occurring during infiltration. High vacuum equipment should be used to prevent magnesium from oxidation.

Finally, future research must also be directed at investigating the effects of interfacial reactions by using transmission electronic microscopy (TEM). The interfacial reactions are expected to enhance wettabilty between Mg and SiC, accelerate infiltration and modify the structure of the matrix upon solidification.

References

1. K. G. Kerider, "*Composite Materials*" Vol. 4 *Metallic Matrix Composite*, Ed. K. G. Kerider, Academic Press, New York and London, 1974
2. J.N. Fridlyander and I. H. Marshall, *Metal Matrix Composites*, First Edition, Cahpman & Hall, London, England, 1995.
3. B. L. Mordike and K. U. Kainer, " Manufacture and Characterization of Magnesium Composite Materials", Trans. Indian Inst. Met. Vol. 50, No. 6, Dec 1997, pp 665-674
4. D. J. Lloyd, "Particle Reinforced Aluminum and Magnesium Matrix Composites", International Materials Review, Vol. 39, No. 1, 1994, pp 1-39
5. C. A. Leon, *Infiltration Processing of Metal Matrix Composites Using Coated Ceramic Particulates* Thesis of PhD, McGill University, 2000
6. S. Rawal, "Metal-Matrix Composites for Space Applications" JOM, 53 (4) (2001), pp 14-17
7. K. U. Kainer, " Influence of the Production Technique and Type of Reinforcement on the Properties of Magnesium-Matrix-Composites", PD-Vol. 37, Composite Material Technology ASME1991, pp 191-197
8. M. Gupta, M. O. Lai and D. Saravanaranganathan, "Synthesis, Microstructure and Properties Characterization of Disintegrated Melt Deposited Mg/SiC Composites", Journal of Materials Science, Vol. 35, 2000, pp 2155-2165
9. T. W. Clyne and P. J. Whiters, *An Introduction to Metal Matrix Composites*, Second Edition, Cambridge University Press, London, England, 1995
10. R. Asthana, P. K. Rohatgi and S. N. Tewari, "Infiltration Processing of Metal-Matrix Composites: A Review", Processing of Advanced Materials, Vol. 2, 1992, pp 1-17
11. M. M. Avedesian and H. Baker, *Magnesium and Magnesium Alloys*, ASM International, 1995

12. H. O. Pieson, *Handbook of Refractory Carbides and Nitrides – Properties, Characteristics, Processing and Applictions,* Noyes Publications, Westwood, New Jersey, USA, 1996

13. H. Hu, " Squeeze Casting of Magnesium Alloys and Their composites", Journal of Materials Science, Vol. 33, 1998, pp 1579-1589

14. T. M. Yue and G. A. Chadwick, "Squeeze Casting of Light Alloys and Their Composites", Journal of materials Processing Technology, Vol. 58, 1996, pp 302-307

15. S. M. Lee, H, Shen and C. P. Hong, "Formation Criterion of Macrosegregation in a Squeeze-cast Al-7mass%Si Alloy", ISIJ International, Vol. 39, 1999, No. 11, pp 1160-1168

16. H. Yamagichi, "Advanced Ceramics and Their Application to Squeeze Casting", Die Casting Engineer, Vo. 40, 1996, No. 3, pp 34-39

17. L. Hu and E. Wang, "Fabrication and Mechanical Properties of SiC_w/ZK51A Magnesium Matrix Composite by Two-step Squeeze Casting", Materials Science and Engineering A278, 2000, pp 267-271

18. A. Okura, "*Mechanical Properties of Metallic Composites (USA)*", Marcel Dekker, Inc., New York, 1994 pp 739-758

19. V. Laurent, P. Jarry and G. Regazzoni, "Processing-Microstrucure Relationships in Compocast Magnesium/SiC", Journal of Materials Science, Vol. 27, 1992, pp 4447-4459

20. M. K. K. OO, P. S. Ling and M. Gupta, " Characteristics of Mg-Based Composites Synthesized Using A Novel Mechanical Disintegration and Deposition Technique", Metallurgical and Materials Transactions A, Vol. 31A, Jul. 2000, pp 1873-1881

21. S. C. V. Lim, M. Gupta and L. Lu, Processing, Microstructure, and Properties of Mg-SiC Composites Synthesized Using Fluxless Casting Process", Materials Science and Technology 2001, 17(7), pp 823-832

22. G. Huard et al., "SiC_p/Mg Composites Made by Low-Energy Mechanical Processing" Canidian Metallurgical Quarterly, Vol. 38, No. 3, 1999, pp 193-200

23. H. Kaneda and T. Choh, "Fabrication of Particulate Reinforced Magnesium Composites by Applying a Spontaneous Infiltration Phenomenon", Journal of Materials Science, Vol. 32, 1997, pp 47-56
24. T. W. Hong et al., "Microstructural Evolution and Semisolid Forming of SiC Particulate Reinforced AZ91HP Magnesium Composites", Materials Science and Technology (UK), Vol. 16, No. 7-8, 2000, pp 887-892
25. S. K. Kim and Y. J. Kim, "Rheological Behavior and Fluidity of SiC_p + AZ91HP Magnesium Composites", Materials Science and Technology (UK), Vol. 16, No. 7-8, 2000, pp 877-881
26. S. K. Kim and Y. J. Kim, " Rotation-Cylinder Method for Fabrication of SiC Particle Reinforced Magnesium Composites", Metals and Materials (South Korea), Vol. 6, No. 4, 2000, pp 359-364
27. C.A. Leon and R.A.L. Drew "Processing of MMCs by Wetting-Assisted Infiltration", Processing & Fabrication of Advanced Materials VII, Eds. T. Srivatsan and K. Khor, TMS Fall Meeting, 1998, pp.323-334
28. J. Hojo, O. Sagawa and H. Kimura, "Sintering of Ni Powder-Coated Al_2O_3 Particles and Metal Infiltration into the Porous Sintered Body", Journal of the Japan Society of Powder and Powder Metallurgy, Vol. 41, No. 10, 1994, pp 1193-1198
29. J. Hojo et al., "Preparation of Nickel-Alumina Composite Using thew Metal-Coated Particles", Journal of the Japan Society of Powder and Powder Metallurgy, Vol. 36, No. 2, 1989, pp 77-80
30. J. Narciso et al., "Wettability of Binary and Ternary Alloys of the System Al-Si-Mg with SiC Particulates", Scripta Metallurgical et Materialia, Vol. 31, No. 11, 1994, pp 1495-1500
31. D. Muscat and R. A. L. Drew, "Modeling the Infiltration Kinetics of Molten Aluminum into Porous Titanium Carbide", Metallurgical and Materials Transactions A, Vol. 25A, Nov 1994, pp 2357-2370
32. D. Muscat, R. L. Harris and R. A. L. Drew, "The Effect of Pore Size on the Infiltration Kinetics of Aluminum in T.C", Acta Metall. Mater. Vol. 42, No. 12, 1994, pp 4155-4163

33. J. A. Dekock and Y. A. Chang, "The Stability of Interface in High-Temperature Metal Matrix Composites", JOM, Vol. 45, No. 3, 1993, pp 21-23
34. Y. Cai, M. J. Tan, G. J. Shen, and H. Q. Su, "Microstructure and Heterogeneous Nucleation Phenomenon in Cast SiC Particles Reinforced Magnesium Composite", Materials Science and Engineering, A282, 2000, pp 232-239
35. Y. Cai, D. Taplin, M. J. Tan and W. Zhou, " Nucleation Phenomenon in SiC Particulate Reinforced Magnesium Composite", Scripta Materialia, Vol. 41, No. 9, 1999, pp 967-971
36. K. N. Braszczynska and A. Bochenek, "Contribution of Silicon Carbide Particles to the Formation of th Structure of Magnesium Cast Composites", Revue de Metallurgie, Cashier D'information Techniques (France), Vol. 97, No. 12, Dec 2000, pp 1455-1462
37. J. Bouix et al., "Physico-chemistry of Interfaces in Inorganic-Matrix Composites", Composites Science and Technology, Vol. 61, 2001, pp 355-362
38. G. D. Zhang, "Interfaces in Metal Matrix Composites", Chinese Journal of materials Research", Vol. 11, No. 6, Dec 1997, pp 649-657
39. B. Inem and G. Pollard, "Interface Structure and Fractography of a Magnesium-alloy, Metal-Matrix Composite Reinforced with SiC Particles", Journal of Materials Science, Vol. 28, 1993, pp 4427-4434
40. O. J. Ilegbusi and J. J. Yang, "Porosity Nucleation in Metal-Matrix Composites", Metallurgical and Materials Transactions A, Vol. 31, Aug 2000, pp 2069-2074
41. L. X. Hu, Y. W. Yang, S. J. Luo and X. Y. Xu, "Investigation on the Kinetics of Liquid Aluminum into an Alumina Fibrous Preform", Journal of Materials Processing Technology, Vol. 94, 1999, pp 237-230
42. T. Yamauchi and Y. Nishida, "Infiltration Kinetics of Fibrous Preform by Aluminum with Solidification", Acta Metallurgical Materials, vol. 43, No. 4, 19995, pp 1313-1321

43. A. Luo, "Processing, Microstructure and Mechanical Behavior of Cast Magnesium Metal Matrix Composites", Metallurgical Materials Transaction A, Vol. 26A, No. 9, 1995, pp 2445-2455
44. T. P. D. Rajan, R. M. Pillai and B. C. Pai, " Review: Reinforcement Coating and Interfaces in Aluminum Metal Matrix Composites", Journal of Materials Science, Vol. 33, 1998, pp 3491-3503
45. B. L. Mordike and P. Lukáč, "Interfaces in Magnesium-based Composites", Surface and Interface Analysis, Vol. 31, 2001, pp 682-691
46. R. Y. Lin, "Composite Interfacial Reactions", JOM, Vol. 45, No. 3, 1993, PP 20
47. M. Manoharan, M. Gupta, M. O. Lai and D. Saravanaranganathan, "Application of Model for Work Hardening Behavior of SiC Reinforced magnesium Based Metal Matrix Composites", Materials Science and Technology (UK), Vol. 16, No. 6, 2000, pp 670-674
48. M. Manoharan, M. Gupta, L. Lu and M. O. Lai, "Technology Reviews and Studies - Application of A Model for the Work Hardening Behavior of SiC Reinforced magnesium Based Metal Matrix Composites", Materials Technology, Vol. 16, No. 3, 2001, pp 187-197
49. R. A. Saravanan and M. K. Surappa, "Fabrication and Characterization of Pure Magnesium – 30 vol.% SiC_p Particle Composite", Materials Science and Engineering, A276, 2000, pp 108-116
50. ASTM C20-97, "Standard Test Method for Apparent Porosity, Water Absorption, Apparent Specific Gravity, and Bulk Density by Boiling Water"
51. G. E. Lucas, G. R. Odette and J. W. Sheckherd, "Shear Punch and Microhardness Tests for Strength and Ductility Measurements", ASTM STP888, 1986, pp 112-140
52. P. Wanjara, R. A. L. Drew, and S. Yue, "Shear Punch Test for Strength and Ductility Measurements of Ti-6Al-4V/TiC Particulate Reinforced MMCs", Titanium' 95. Vol. III, Birmingham, UK, Oct 1995, pp 2851-2858

53. B. S. Murty, S. K. thakur and B. K. Dhindaw, "On the Infiltration Behavior of Al, Al-Li and Mg Melts through SiC_p Bed", Metallurgical and Materials Transactions A (USA), Vol. 31A, No. 1 Jan 2000, pp 319-325

54. J. Jackowski and J. Grabian, "Porosity of Metal Infiltrated Composites – An Attempt at the Problem Analysis", Science and Engineering of Composite Materials, Vol. 9, No. 1, 2000, pp 17-24

55. R. J. Arsenault and N. Shi, "Dislocation Generation Due to Differences between the Coefficients of Thermal Expension", Materials Science and Engineering, ol. 81, 1986, pp 175-187